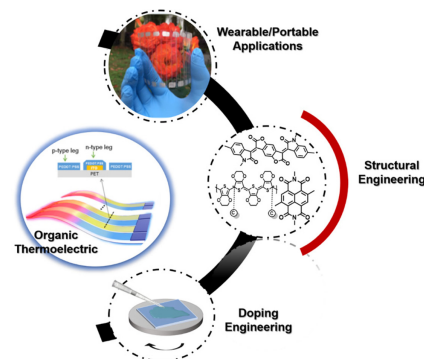


# Recent Progress in Organic Thermoelectric Materials and Devices

Soonyong Lee<sup>†,1</sup>Soohyun Kim<sup>†,2</sup>Ambika Pathak<sup>1</sup>Ayushi Tripathi<sup>1</sup>Tian Qiao<sup>2</sup>Yeran Lee<sup>1</sup>Hyunjung Lee<sup>\*,2</sup>Han Young Woo<sup>\*,1</sup><sup>1</sup> Department of Chemistry, College of Science, Korea University, 145 Anam-ro, Seongbuk-gu, Seoul 02841, Korea<sup>2</sup> School of Advanced Materials Engineering, Kookmin Univ., Jeongneung-ro 77, Seongbuk-gu, Seoul 02707, Korea

Received March 20, 2020 / Revised April 23, 2020 / Accepted April 28, 2020

**Abstract:** In recent years, thermoelectric (TE) devices have attracted a growing attention due to their promising ability to convert waste heat into readily available electric energy. Compared to inorganic counterparts, organic TE devices emerged as the potential candidates for room-temperature and flexible (even wearable) TE power generation. During last few decades, extensive studies have been performed on the p- and n-type materials and devices to build up the inter-relationship among the TE parameters (*i.e.*, electrical conductivity, Seebeck coefficient, thermal conductivity and power factors), demonstrating a great potential of organic TEs. In this review, recent progresses in the organic TE materials and devices, dopants and doping method, charge transport models and flexible TE device applications are summarized and the key strategies and future prospects to further optimize TE performance are discussed.



**Keywords:** organic thermoelectrics, waste heat, Seebeck coefficient, conductivity, power factor.

## 1. Introduction

The use of renewable energy sources is becoming imperative owing to global warming and the shortage of fossil fuel reserves.<sup>1</sup> Heat is an abundant source of energy, but is often wasted irrespective of whether it originates from natural sources like solar and geothermal sources or artificial sources like motor vehicles and the industrial sector.<sup>2</sup> If heat from one of these sources is brought into contact with certain conductors or semiconductors, an electric current can be generated as a result of the potential difference, which develops because of temperature gradient. This phenomenon was discovered by Thomas J. Seebeck in 1821 and is termed the Seebeck effect.<sup>3</sup> The conversion of electrical energy to thermal energy is known as the Peltier effect, which was discovered by Jean Peltier (1834),<sup>4</sup> and can be employed for spot cooling or heating applications. Therefore, thermoelectric (TE) devices are attractive candidates for solving the energy problem by means of harvesting waste heat and solar thermal energy and are also useful for health monitoring sensors that employ body heat. The performance of TE materials is generally expressed by a dimensionless thermoelectric figure of merit ZT,<sup>5–7</sup>

$$ZT = \frac{\alpha^2 \sigma T}{k} \quad (1)$$

where  $\alpha$  is the Seebeck coefficient,  $\sigma$  is electrical conductivity,  $k$  is thermal conductivity, and  $T$  is the temperature. The power factor (PF), expressed as  $PF = \alpha^2 \sigma$ , is often used to compare the energy conversion capabilities among different materials in organic TEs. However, the possibility of improving the PF is limited owing to the interdependence and coupling between the two major parameters, the  $\alpha$  and  $\sigma$ . As  $\alpha$  and  $\sigma$  are strongly and oppositely dependent on the carrier concentration associated with the electronic structure of the materials, these two parameters need to be fine-modulated to optimize the resulting PF.

So far, inorganic materials like bismuth telluride ( $Bi_2Te_3$ ), tin selenide ( $SnSe$ ), lead telluride ( $PbTe$ ), and silicon-germanium ( $SiGe$ ) have been investigated for their TE properties.<sup>8–11</sup> These materials have been employed in TE devices with a high figure of merit ( $ZT > 2$ ),<sup>12</sup> and successfully commercialized. Despite their high performance, these materials have several disadvantages such as their high cost, toxicity, high thermal conductivity much larger than  $1 \text{ W m}^{-1} \text{ K}^{-1}$ ,<sup>13</sup> and processing difficulties. Conversely, organic materials offer more cost-effective high-throughput fabrication using solution-based printing techniques with the additional advantages such as facile tunability of molecular structures to tailor the properties, low temperature energy harvesting and temperature sensing, *etc.* Organic materials are flexible and robust with low weight and low thermal conductivity ( $0.1$ – $0.8 \text{ W m}^{-1} \text{ K}^{-1}$ ).<sup>14</sup> Therefore, organic TE materials have been identified as an alternative to find complementary applications of inorganic TE materials and considerable efforts have been devoted

**Acknowledgments:** This work was supported by the National Research Foundation (NRF) of Korea (Grants NRF-2019R1A2C2085290, 2019-R1A6A1A11044070, 2017R1A2B2010552, and 2015R1A5A7037615).

**\*Corresponding Authors:** Hyunjung Lee (hyunjung@kookmin.ac.kr), Han Young Woo (hywoo@korea.ac.kr)

<sup>†</sup>S. Lee and S. Kim contributed equally to this work.

to enhance their TE performance. Despite all the aforementioned advantages, the development of efficient organic TE materials is hampered by the low carrier mobility and mediocre  $\alpha$ . However, ongoing efforts involving the development of doping strategies and structural design have proved helpful to attain high ZT values of 1.02 and 0.2 for p- and n-type TE materials, respectively.<sup>15-17</sup> Organic TE materials and devices have great potential as a sustainable power source, *i.e.*, room temperature (or low temperature) TE energy harvesting for flexible (or wearable) electronic devices. Considerable effort has been made to adopt different doping strategies and to design potential building blocks for organic TE materials. In this review, we discuss recent outcomes in the field of p- and n-type organic thermoelectric materials, developments of dopants and doping methods, modelling of charge transport in organic TE materials and flexible TE device (or module) applications, and highlight the approaches that have been proposed and employed to increase the  $\sigma$ ,  $\alpha$ , and PF.

## 2. Organic Thermoelectric Materials

### 2.1. p-Type Thermoelectric Materials

An extensively studied p-type TE material is poly(3,4-ethylenedioxythiophene):poly(styrene sulfonate) (PEDOT:PSS). Its facile processability and stability when heavily doped have resulted in the positively doped PEDOT with PSS counterions being considered as the most promising conducting polymer for TE applications. In-depth research has been conducted to enhance its TE performance, mainly by optimizing dopants and doping methodologies in an attempt to maximize the PF. Excess PSS, which acts as an insulator in PEDOT:PSS films, limits charge carrier transport, resulting in the  $\sigma$  of  $0.012\text{-}17 \text{ S cm}^{-1}$  and PF of  $0.0016\text{-}0.9 \mu\text{W m}^{-1} \text{ K}^2$ .<sup>18</sup> Various studies have attempted to optimize the electrical properties of PEDOT:PSS, for example, introduction of a polar solvent such as dimethylsulfoxide (DMSO) facilitates phase segregation by weakening the Coulombic attraction between the positively charged PEDOT and negatively charged PSS *via* a screening effect, thus obtaining high  $\sigma$ . Furthermore, post-treatments have been reported to modulate the phase segregation of PEDOT:PSS and structural change of the PEDOT chains to that of a quinoid structure.

Crispin *et al.* tried to control the oxidation level of PEDOT:PSS by fabricating electrochemical transistors. By applying high gate voltage to the PEDOT:PSS film, they succeeded in increasing  $\alpha$  whereas  $\sigma$  decreased with reduced carrier concentration. They obtained a maximum PF of  $23.5 \mu\text{W m}^{-1} \text{ K}^2$  with  $\sigma$  in the range of  $0.3\text{-}300 \text{ S cm}^{-1}$  and  $\alpha$  in the range of  $20\text{-}400 \mu\text{V K}^{-1}$  when the doping level was lowered from 33% to 14.5%.<sup>19</sup> In 2013, Luo *et al.* reported the effects of post-treatment, which included the addition of DMSO to a PEDOT:PSS solution, followed by spin casting and post-treatment of the thin PEDOT:PSS film with a mixture of DMSO and the ionic liquid (IL), 1-ethyl-3-methylimidazolium tetrafluoroborate (EMIM-BF<sub>4</sub>). Primarily, the addition of DMSO to PEDOT:PSS resulted in an interconnected network with elongated PEDOT grains, resulting in a maximum PF of  $30.1 \mu\text{W m}^{-1} \text{ K}^2$  with  $\sigma = 930.41 \text{ S cm}^{-1}$  and  $\alpha = 17.99 \mu\text{V K}^{-1}$ . In addition, post-treatment with EMIMBF<sub>4</sub> induced an intercon-

nected network of short and circular PEDOT grains with increased polaron density, resulting in further improvement in  $\alpha$  to maximize the PF ( $38.46 \mu\text{W m}^{-1} \text{ K}^2$ ).<sup>20</sup> Likewise, Pipe *et al.* reported the mixing of PEDOT:PSS with ethylene glycol (EG)/DMSO followed by immersion in an EG solution. This method successfully thinned out the PSS layer, which enhanced the charge carrier mobility ascribed to the reduced tunneling distance between the conductive domains. Their approach increased both  $\sigma$  and  $\alpha$ , and suppressed the thermal conductivity from 0.30 to 0.22  $\text{W m}^{-1} \text{ K}^{-1}$  in the DMSO-mixed PEDOT:PSS and from 0.32 to 0.23  $\text{W m}^{-1} \text{ K}^{-1}$  in EG-mixed PEDOT:PSS.<sup>21</sup> Similarly, Kim *et al.* reported a post-treatment method that entails applying a coating consisting of a mixture of DMSO and hydrazine (as a reducing agent) to a PEDOT:PSS film, reducing the bipolarons into polarons or neutral states in the PEDOT chains, with the benefit of enhancing the  $\alpha$  values. By controlling the concentration of hydrazine (0.0175 wt%), the film exhibited the maximum PF of  $112 \mu\text{W m}^{-1} \text{ K}^2$  with  $\sigma$  of  $578 \text{ S cm}^{-1}$  and  $\alpha$  of  $67 \mu\text{V K}^{-1}$ .<sup>22</sup> Furthermore, Gong *et al.* reported a post-treatment method using DMSO and poly(ethylene oxide) (PEO) which led to both  $\sigma$  and  $\alpha$  increasing simultaneously. The addition of PEO, which strongly interacts with PEDOT, increased the bipolarons in the PEDOT backbone. The formation of increased bipolaron states, which was confirmed by Raman and X-ray photoelectron spectroscopy, enhanced the delocalization of charge carriers on the conjugated backbone and thus increased the  $\sigma$ . In addition, the distribution of the logarithm of density of states (DOS) is highly asymmetric at the Fermi level ( $E_F$ ) for PEDOT in the bipolaron states. Here  $\alpha$  is proportional to the derivative of DOS at  $E_F$  and the increased  $\alpha$  values were obtained from the doped PEDOT:PSS films with enhanced ratios of PEDOT in the bipolaron state. They thus measured  $\sigma$  of  $1061 \text{ S cm}^{-1}$  and  $\alpha$  of  $38.4 \mu\text{V K}^{-1}$  at the maximum PF of  $157.4 \mu\text{W m}^{-1} \text{ K}^2$ , when PEDOT:PSS was doped with 5% DMSO and 0.3% PEO.<sup>23</sup> Ouyang *et al.* reported the sequential treatment of the PEDOT:PSS film with acid ( $\text{H}_2\text{SO}_4$ ) and base ( $\text{NaOH}$ ) to increase both the  $\alpha$  and  $\sigma$  values. The treatment with acid facilitated the charge transport with enhanced  $\sigma$  and treatment with the base dedoped the PEDOT and localized the positive charges, lowering the charge concentration with enhanced  $\alpha$ . The maximum PF of  $334 \mu\text{W m}^{-1} \text{ K}^2$  with  $\sigma$  of  $2170 \text{ S cm}^{-1}$  and  $\alpha$  of  $39.2 \mu\text{V K}^{-1}$ , were obtained by carefully adjusting the treatment with acid and base at room temperature.<sup>24</sup> In 2018, Ouyang and coworkers also reported post-treatments using a series of ILs, 1-ethyl-3-methylimidazolium dicyanamide (EMIM-DCA), 1-ethyl-3-methylimidazolium bis(trifluoromethylsulfonyl)imide (EMIM-TFSI) and EMIM-BF<sub>4</sub> on the PEDOT:PSS surface. The accumulation of cations on the cold side while enhancing the mean hole energy, led to an increase in  $\alpha$ . Using EMIM-DCA, they achieved the maximum PF of  $754 \mu\text{W m}^{-1} \text{ K}^2$  and ZT of 0.75. The TE performance is also competitive against highly functioning inorganic TE materials such as bismuth telluride.<sup>16</sup>

In addition to various post treatments of PEDOT:PSS films, different counterions to replace PSS, such as perchlorate ( $\text{ClO}_4^-$ ), hexafluorophosphate ( $\text{PF}_6^-$ ), bis(trifluoromethylsulfonyl)imide (TFSI),<sup>25</sup> and tosylate (Tos), have been also introduced to optimize the thermoelectric properties. Crispin *et al.* added PEDOT:Tos to the reducing agent, tetrakis(dimethylamino)ethylene (TDAE),

in the vapor state for different periods of time to adjust the oxidation level. TDAE formed a salt with the Tos anions by supplying electrons to oxidized PEDOTs. The salt was further removed by rinsing the films with water. Thereby, the oxidation level was varied between 9 and 36%. At the optimal oxidation level of 22%, a maximum PF of  $324 \mu\text{W m}^{-1}\text{K}^2$  was achieved, resulting in a ZT of 0.25 at room temperature.<sup>26</sup> Kim *et al.* introduced PP-PEDOT:Tos (PP-PEDOT: prepared from a mixture of pyridine and triblock copolymer, poly(ethylene glycol)-block-poly(propylene glycol)-block-poly(ethylene glycol), (PEG-PPG-PEG)) to use as electrodes where the oxidation level of the deposited polymer could be adjusted by applying an electrical potential. The optimized films exhibited  $\sigma$  of  $117 \text{ S cm}^{-1}$  and  $\alpha$  of  $930 \mu\text{V K}^{-1}$ , leading to an unprecedented maximum PF of  $1270 \mu\text{W m}^{-1}\text{K}^2$  with a high ZT value of 1.02.<sup>17</sup> Furthermore, Crispin *et al.* demonstrated a PEDOT transition from the Fermi glass (PEDOT:PSS) to a semi-metal with the Tos counterion (PEDOT:Tos). After treating the film with PEG-PPG-PEG, the grazing-incidence wide-angle X-ray scattering (GIWAXS) study showed that the PEDOT:Tos exhibited a well-ordered crystalline pattern compared to PEDOT:PSS. The introduction of Tos ions enabled them to maximize  $\alpha$  and  $\sigma$  at  $55 \mu\text{V K}^{-1}$  and  $1500 \text{ S cm}^{-1}$  at room temperature, respectively.<sup>27</sup>

Overall, PEDOT derivatives have been extensively studied as the most promising p-type TE material; however, their shortcomings, such as the hygroscopic and acidic properties and the insulating counterions of PSS motivated researchers to broaden their scope to develop new p-type TE polymers. Primarily, researchers investigated the thermoelectric properties of other p-type molecules that were previously shown to exhibit superior charge transport characteristics for organic thin-film transistors and solar cells. Several highly performing TE polymers have been designed based on the poly(2,5-bis(3-alkylthiophen-2-yl)thieno[3,2-*b*]thiophene) (PBTTT) structure, with a highly ordered morphology in film owing to its liquid crystalline nature.<sup>28</sup> Earlier papers reported that PBTTT-C<sub>14</sub> (with tetradecyl side-chains), obtained by immersion doping using a nitrosonium hexafluorophosphate (NO<sub>PF</sub><sub>6</sub>) dopant, yielded a maximum PF of  $1 \mu\text{W m}^{-1}\text{K}^2$ , and PBTTT-C<sub>12</sub> (with dodecyl side-chains), obtained by immersion doping with Fe(III) bis(trifluoromethylsulfonyl)imide [Fe(TFSI)<sub>3</sub>], yielded a maximum PF of  $14 \mu\text{W m}^{-1}\text{K}^2$ .<sup>29</sup> Chabiny *et al.* studied the effect of the different dopants 4-ethyl-benzenesulfonic acid (EBSA) and (tridecafluoro-1,1,2,2-tetrahydrooctyl)-trichlorosilane (FTS) on PBTTT-C<sub>14</sub> films. Even though the value of  $\sigma$  that was achieved by using EBSA ( $1300 \text{ S cm}^{-1}$ ) via solution doping was higher than that of FTS ( $1000 \text{ S cm}^{-1}$ ) via vapor doping, the vapor-doped PBTTT-C<sub>14</sub>:FTS film had a maximum PF of  $110 \mu\text{W m}^{-1}\text{K}^2$ . They observed that the strongly amorphous character resulting from FTS doping had little effect on the conductivity while greatly increasing the value of  $\alpha$ . Moreover, they postulated that the disordered region may have led to strongly perturbed DOS, thus, enhancing  $\alpha$ .<sup>30</sup> Later, Chabiny and coworkers investigated the TE characteristics of PBTTT-C<sub>14</sub> by doping with 2,3,5,6-tetrafluoro-7,7,8,8-tetracyanoquinodimethane (F4TCNQ) and 2,5-difluoro-7,7,8,8-tetracyanoquinodimethane (F2TCNQ) in the vapor and solution states. In the vapor-doped polymer films with F4TCNQ, an elongated orientation correlation length (OCL) was observed

using resonance soft X-ray scattering (RSoXS). Increased OCL can be correlated with charge carrier mobility ( $\mu$ ) and the improvement of  $\sigma$  without significantly affecting  $\alpha$ . Therefore, the vapor-doped PBTTT-C<sub>14</sub> with F4TCNQ exhibited the maximum PF of  $120 \mu\text{W m}^{-1}\text{K}^2$  with of  $670 \text{ S cm}^{-1}$  and of  $42 \mu\text{V K}^{-1}$  whereas doping with F2TCNQ yielded maximum PF of  $70 \mu\text{W m}^{-1}\text{K}^2$ .<sup>31</sup>

Another widely studied p-type polymer is poly(3-hexylthiophene) (P3HT). Its regio-regular arrangement of side-chains allows efficient  $\pi$ - $\pi$  stacking of the conjugated backbones with pronounced charge carrier transport properties. For example, Zhu *et al.* reported that P3HT film doped with Fe(III) (TFSI)<sub>3</sub> achieved a maximum PF of  $26 \mu\text{W m}^{-1}\text{K}^2$  at temperatures between 300 and 340 K, which was attributed to its high carrier concentration ( $1.62 \times 10^{21} \text{ cm}^{-3}$ ).<sup>32</sup> In addition, to improve the PF by utilizing different doping methods, Jang *et al.* prepared P3HT:FeCl<sub>3</sub> films by wire bar coating. This method improved the intermolecular chain packing, yielding high  $\sigma$  ( $254 \text{ S cm}^{-1}$ ) and a maximum PF of  $35 \mu\text{W m}^{-1}\text{K}^2$ .<sup>33</sup> In 2017, Cho *et al.* compared the TE properties of P3HT and a diketopyrrolopyrrole (DPP)-based polymer (PDPP3T) by drop-cast sequential doping with FeCl<sub>3</sub>. The maximum PF values were determined to be  $56 \mu\text{W m}^{-1}\text{K}^2$  for P3HT and  $276 \mu\text{W m}^{-1}\text{K}^2$  for PDPP3T, respectively. Electron delocalization in the backbone, enhanced intramolecular charge-transport, and large polarizability induced by the donor-acceptor (D-A) structure of the PDPP3T resulted in the conformation being preserved after doping, which influenced the hopping and carrier transport process between the conjugated polymer chains.<sup>34</sup>

Leclerc *et al.* reported a series of carbazole-based D-A polymers, poly[N-9'-heptadecanyl-2,7-carbazole-*alt*-5,5'-(4',7'-di-2-thienyl-2',1',3'-benzothiadiazole)] (PCDTBT), poly[N-9'-heptadecanyl-2,7-carbazole-*alt*-5,5'-(2,2'-bithiophene)] (PCDT), and poly[N-9'-heptadecanyl-2,7-carbazole-*alt*-5,5'-(2,2'-(1,4-phenylene)dithiophene)] (PCDTB). Addition of planar moieties such as benzene and benzothiadiazole (BT) units to PCDTB and PCDTBT were shown to increase the crystalline morphology by increasing the interchain interaction, thus facilitating charge carrier transport. After doping with FeCl<sub>3</sub>, PCDTBT showed the maximum  $\sigma$  of  $500 \text{ S cm}^{-1}$  and PF of  $19 \mu\text{W m}^{-1}\text{K}^2$ , which is higher than those of PCDT (PF =  $6.5 \mu\text{W m}^{-1}\text{K}^2$ ) and PCDTB (PF =  $14 \mu\text{W m}^{-1}\text{K}^2$ ).<sup>35</sup>

Systematic variation of the heteroaromatic moieties incorporated in the conjugated polymeric main chain has been proven to be effective to tune the electronic structure and intermolecular packing interactions. Yee *et al.* reported a series of FeCl<sub>3</sub>-doped poly(3-alkylchalcogenophene) (P3RT) derivatives, P3RS, P3RSe, and P3RTe (where R is 3,7-dimethyloctyl). The optical band gaps decreased as the heteroatom of the chalcogen changed from S through Se to Te. They additionally observed an increase in  $\sigma$  as the heteroatom changed from P3RS ( $4 \text{ S cm}^{-1}$ ) to P3RSe ( $29 \text{ S cm}^{-1}$ ) to P3RTe ( $46 \text{ S cm}^{-1}$ ) at  $[\text{FeCl}_3] = 1 \times 10^{-3} \text{ M}$ . However, at a higher concentration of  $[\text{FeCl}_3] = 5 \times 10^{-3} \text{ M}$ , the P3RS and P3RSe polymers exhibited higher  $\sigma$  ( $17$  and  $52 \text{ S cm}^{-1}$ ) compared to P3RTe ( $\sigma = 14 \text{ S cm}^{-1}$ ). As a result, at  $[\text{FeCl}_3] = 5 \times 10^{-3} \text{ M}$ , P3RT and P3RSe achieved higher maximum PF of  $12$  and  $13 \mu\text{W m}^{-1}\text{K}^2$ , compared to P3RTe.<sup>36</sup> Similarly, Zhu *et al.* reported a Se-substi-

tuted DPP derivative (PDPPSe-12) using  $\text{FeCl}_3$  as dopant. The introduction of the Se atom induced efficient intermolecular packing *via* Se-Se chalcogen interactions and the enhanced intermolecular packing increased  $\sigma$  while sustaining its morphology after the dopants were intercalated into the polymer domains. The hole mobility  $\mu$  of PDPPSe-12 increased to  $1.87 \text{ cm}^2 \text{ V}^{-1} \text{ s}^{-1}$  at  $[\text{FeCl}_3] = 5 \text{ mM}$  and was maintained at  $1.10 \text{ cm}^2 \text{ V}^{-1} \text{ s}^{-1}$  even when the dopant concentration was  $[\text{FeCl}_3] = 15 \text{ mM}$  compared to PDPPS-12 at the same dopant concentrations ( $0.92\text{--}0.22 \text{ cm}^2 \text{ V}^{-1} \text{ s}^{-1}$ ). As a result, PDPPSe-12 exhibited maximum  $\sigma$  of  $997 \text{ S cm}^{-1}$  at  $[\text{FeCl}_3] = 16 \text{ mM}$  whereas that of PDPPS-12 was  $318 \text{ S cm}^{-1}$  at  $[\text{FeCl}_3] = 14 \text{ mM}$ . The maximum PF of  $300 \mu\text{W m}^{-1}\text{K}^2$  was achieved for PDPPSe-12 at room temperature, which was twice as high as that of PDPPS-12 ( $126 \mu\text{W m}^{-1}\text{K}^2$ ). Moreover, PDPPSe-12 yielded the maximum PF of  $364 \mu\text{W m}^{-1}\text{K}^2$  at  $55^\circ\text{C}$ , which is attributed to the combination of thermally activated hopping and dopant-induced ion scattering.<sup>37</sup>

Diversification of the structural modifications and doping methodology has enabled the successful optimization of the thermoelectric parameters, particularly in terms of the  $\sigma$ . However, further investigations are required to tune the  $\alpha$ . Systematic approaches have been performed to resolve the trade-off between the  $\alpha$  and  $\sigma$ . For example, Azoulay *et al.* synthesized a proquinoidal thiadiazoloquinoxaline (TQ)-based polymer, poly(4-(4,4-dihexadecyl-4H-cyclopenta[2,1-*b*:3,4-*b'*]dithiophen-2-yl)-6,7-dimethyl[1,2,5]-thiadiazolo[3,4-*g*]quinoxaline) (PCQ). The open-shell electronic ground state of this compound yielded a  $\sigma$  of  $\sim 10^3 \text{ S cm}^{-1}$  and large  $\alpha$  ( $> 1000 \mu\text{V K}^{-1}$ ) for the pristine film. The use of an open-shell dopant, the galvinoxyl radical (Gav), increased  $\sigma$  by  $\sim 100$ -fold while minimally impacting the value of  $\alpha$  (it decreased by a factor of  $\sim 2$ ), yielding the optimal PF of  $> 10 \mu\text{W m}^{-1}\text{K}^2$ .<sup>38</sup> Similarly, Xu *et al.* synthesized a series of 2,6-dialkyl-benzo[1,2-*d*;4,5-*d'*]bistriazole (BBTa26)-based proquinoidal conjugated polymers pBBTa26-2T (containing dithiophene), pBBTa26-4T (tetrathiophene), pBBTa26-TT (thieno[3,2-*b*]thiophene), and pBBT26a-BDT (benzodithiophene). Because of the proquinoidal character of all four polymers, they showed high  $\sigma$  values of  $10^{-5}$  to  $10^{-2} \text{ S cm}^{-1}$  in the neat film without doping. Specifically, pBBTa26-TT exhibited an exceptionally high  $\sigma$  of  $10^{-2} \text{ S cm}^{-1}$  owing to the small dihedral angle ( $0.1\text{--}0.2^\circ$ ) of its backbone. Despite the amorphous and face-on oriented morphology, a maximum  $\sigma$  of  $102.1 \text{ S cm}^{-1}$  was obtained for pBBTa26-TT by sequential doping with a solution of F4TCNQ. The highly intra-chain-delocalized polarons were responsible for the increase in  $\sigma$ . Even though  $\alpha$  is inversely related to  $\sigma$ , the simultaneous enhancement of  $\alpha$  and  $\sigma$  could be made to occur *via* carrier-induced softening induced by delocalized polarons, and the resulting maximum PF of  $6.8 \mu\text{W m}^{-1}\text{K}^2$  was obtained for pBBTa26-TT. Interestingly, the  $\pi$ -spacer 2T containing pBBTa26-2T with maximum  $\sigma$  of  $43.1 \text{ S cm}^{-1}$  showed remarkably high PF of  $11.8 \mu\text{W m}^{-1}\text{K}^2$ .<sup>39</sup> The conductivity can be increased by increasing the charge carrier concentration. In addition, it would be possible to boost  $\mu$  and  $\sigma$  by optimizing the morphology of the crystalline film. Woo *et al.* reported a series of polypyrrole (PPy) films that were ionically interconnected *via* two-monomer-connected-precursor polymerization by various diacid linkers. Variation of these linkers enabled the film morphology and electrical properties to be successfully modulated. The PPy-Nap polymer

with 1,5-naphthalenedisulfonic acid as a fused aromatic linker exhibited a higher  $\sigma$  ( $\sim 78 \text{ S cm}^{-1}$ ) than that ( $6.7 \text{ S cm}^{-1}$ ) of the reference PPy without a linker (PPy-ref) and the resulting PF of PPy-Nap was higher than that of PPy-ref ( $0.21 \text{ vs. } 0.043 \mu\text{W m}^{-1}\text{K}^2$ ). This can be attributed to the  $\mu$  of PPy-Nap being approximately five times higher owing to its tighter cofacial  $\pi\text{-}\pi$  stacking and crystalline morphology compared to PPy-ref. All PPys had similar charge carrier concentrations with similar  $\alpha$  ( $5\text{--}8 \mu\text{V K}^{-1}$ ). This study suggested that both  $\sigma$  and PF could be increased while maintaining  $\alpha$  by enhancing the ordered conductive domains and  $\mu$  at the same doping level.<sup>40</sup>

Xu *et al.* also reported two high-spin proquinoid benzo[1,2-*c*;4,5-*c'*]bisthiadiazole (BBT)-based polymers, pBBT-2T-TT and pBBT-2T-2T, which contain TT and 2T as  $\pi$ -spacers, respectively. The strong quinoid character of the BBT polymers allowed efficient intramolecular delocalization of the polarons/bipolarons and intermolecular long-range ordering. Extensive intra- and intermolecular delocalization of the polarons/bipolarons also led to a large increase in  $\alpha$  *via* carrier-induced softening. The use of sequential solution doping using  $\text{FeCl}_3$  as p-dopant resulted in the maximum being determined to be  $287 \text{ S cm}^{-1}$  and  $313.9 \text{ S cm}^{-1}$  for pBBT-2T-TT and pBBT-2T-2T, respectively. Interestingly, density functional theory and variable temperature electron paramagnetic resonance (VT-EPR) spectroscopy were used to calculate that pBBT-2T-TT possesses triplet bipolarons. The triplet bipolarons can induce the high  $\alpha$  value *via* the spin entropy contribution. The formation of triplet bipolarons in pBBT-2T-TT was rationalized on the basis of its larger  $\alpha$  despite its high  $\sigma$ . By controlling the level of doping, the maximum PF of  $65.2 \mu\text{W m}^{-1}\text{K}^2$  with  $\sigma$  of  $232.7 \text{ S cm}^{-1}$  and  $\alpha$  of  $49.4 \mu\text{VK}^{-1}$  of pBBT-2T-TT was higher than the PF obtained for pBBT-2T-2T (PF =  $43.5 \mu\text{W m}^{-1}\text{K}^2$ ).<sup>41</sup> Jang *et al.* reported two different cyclopentadithiophene (CDT)-based polymers, PCDTFBT and PCDTPT, which contained fluorinated benzothiadiazole (FBT) and pyridinethiadiazole (PT), respectively. They used D-A molecular design to tune the highest occupied molecular orbital (HOMO)-lowest unoccupied molecular orbital (LUMO) levels over a wide range. The HOMO levels they obtained for both molecules were appropriate such that doping with F4TCNQ induced efficient charge transfer. Moreover, the long side-chains of these molecules were responsible for retaining their good solubilities even at high dopant contents (up to 38 mol%). This permitted the preparation of uniform polymer:dopant films for which maximum PF of  $31.5 \mu\text{W m}^{-1}\text{K}^2$  and  $21.8 \mu\text{W m}^{-1}\text{K}^2$  was eventually obtained for PCDTFBT and PCDTPT, respectively.<sup>42</sup>

Additionally, side-chain engineering (*i.e.*, the chain length, structure, and branch point in the solubilizing alkyl side-chains) presents an efficient way to adjust the intermolecular packing in the solid state as well as in solution, yielding different charge transport and TE characteristics. For instance, PDPP(2-OD)<sub>2</sub>TT, comprised of alternating DPP and TT moieties with 2-octyldodecyl substituents, was well characterized for organic thin film transistor (OTFT) applications, showing a hole mobility ( $\mu_h$ ) of 1 to  $10 \text{ cm}^2 \text{ V}^{-1} \text{ s}^{-1}$ . Kiriy *et al.* modified the side-chains by extending the branching point (6-octyldodecyl) to synthesize PDPP(6-OD)<sub>2</sub>TT with the aim of improving the solubility and crystallinity of the film and studied its TE performance by using the two different dopants F4TCNQ and hexacyanotrimethylenecyclopropane

(CN6-CP). In this report, the maximum conductivity of the PDPP(6-DO)<sub>2</sub>TT:F4TCNQ films was  $10^2 \text{ S cm}^{-1}$  whereas that of the PDPP(6-DO)<sub>2</sub>TT:CN6-CP films was superior ( $70 \text{ S cm}^{-1}$ ). This difference was attributed to more effective doping with CN6-CP compared to F4TCNQ as the LUMO (-5.87 eV) level of CN6-CP is positioned below the HOMO level of PDPP(6-DO)<sub>2</sub>TT (-5.5 eV), offering a feasible charge transfer process.<sup>43</sup> Muller *et al.* focused on improving the processability of the polymer and reported the p(g<sub>4</sub>T-TT) polymer, which consists of a rigid bithiophene-thienothiophene (2T-TT) backbone with tetraethylene glycol side-chains on the bithiophene moiety. This improved the compatibility of the polymer and dopant, promoting coprocessing and morphologically stable polymer:dopant blends. The electron-donating tetraethylene glycol side-chains of the p(g<sub>4</sub>T-T) polymer decreased the ionization energy, thus making it possible to use even weaker dopants, *i.e.*, 3-dichloro-5,6-dicyano-1,4-benzoquinone (DDQ). As a result, for both F4TCNQ and DDQ, a  $\sigma$  of  $100 \text{ S cm}^{-1}$  was achieved, demonstrating that side-chain engineering has a critical influence on the film morphology, charge carrier transport, and resulting TE properties.<sup>44</sup> Woo *et al.* reported a

new D-A type conjugated polymer, poly[(4,4'-(bis(hexyldecylsulfanyl)methylene)cyclopenta[2,1-*b*:3,4-*b'*]-dithiophene)-*alt*-(benzo[*c*][1,2,5]thiadiazole)] (PCPDTSBT), which is based on CDT-benzothiadiazole (BT) units and with the normal alkyl side-chains replaced with bis(alkylsulfanyl)methylene substituents. The introduction of sp<sup>2</sup>-hybridized side-chains and sulfur-sulfur (S-S) chalcogen interactions successfully enhanced the chain planarity and crystalline interchain packing. Moreover, when the polymer was doped with 9 mol% of B(C<sub>6</sub>F<sub>5</sub>)<sub>3</sub>, it exhibited the maximum  $\sigma$  ( $7.47 \text{ S cm}^{-1}$ ), which was about one order of magnitude higher than that of PCPDTBT ( $0.65 \text{ S cm}^{-1}$ ) with normal ethylhexyl side-chains. Finally, the maximum PF of PCPDTSBT,  $7.73 \text{ W m}^{-1} \text{ K}^{-2}$ , is higher than that ( $4.41 \mu\text{W m}^{-1} \text{ K}^{-2}$ ) of PCPDTBT.<sup>45</sup> The molecular structures of aforementioned p-type thermoelectric materials and their thermoelectric characteristics are summarized in Figure 1 and Table 1.

## 2.2. n-Type Thermoelectric Materials

Although extensive studies on p-type TE materials and dop-

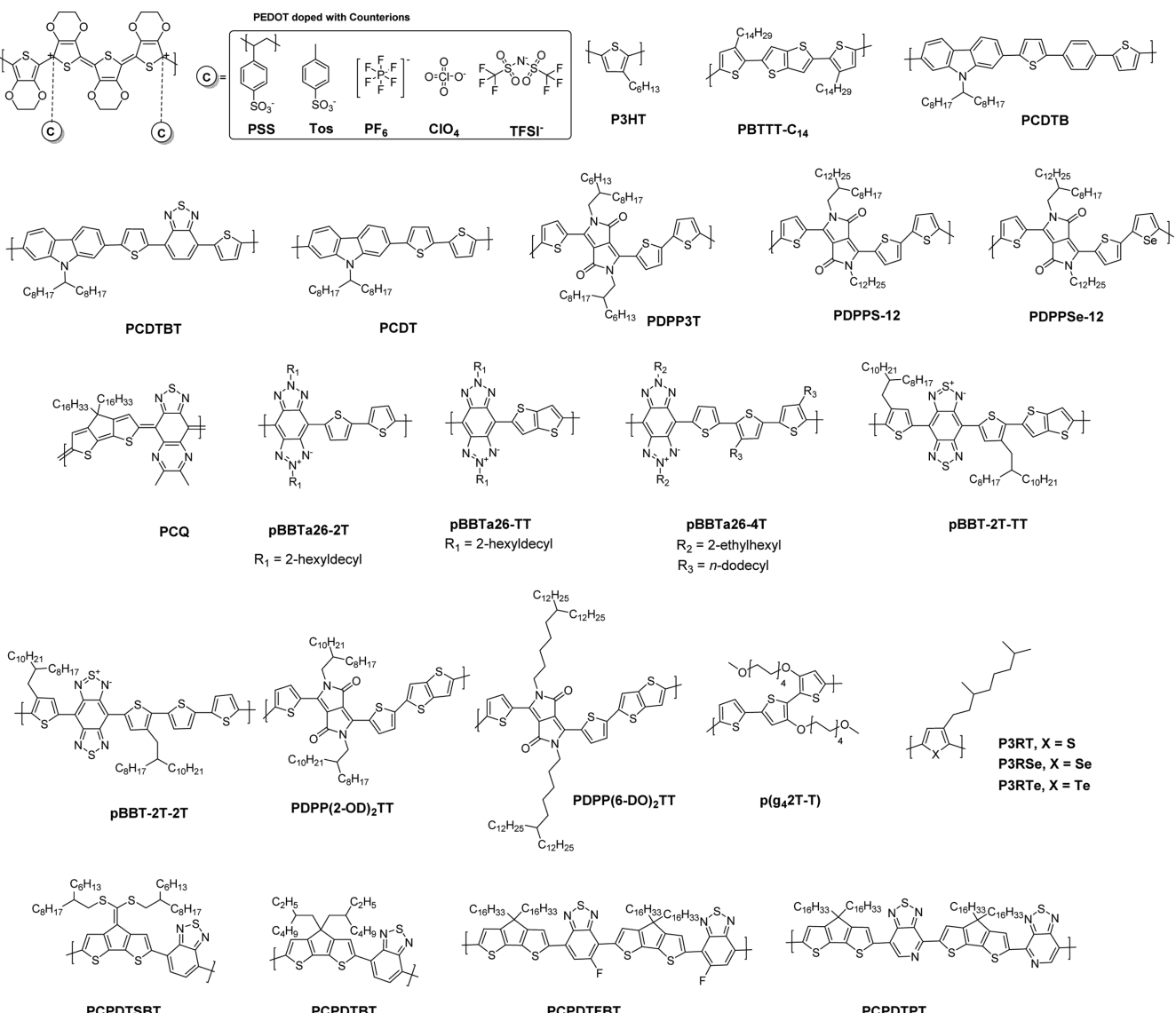


**Figure 1.** Chemical structures of p-type TE materials.

**Table 1.** Summary of TE properties of p-type conjugated molecules. The value in parenthesis is the maximum  $\alpha$  or  $\sigma$ 

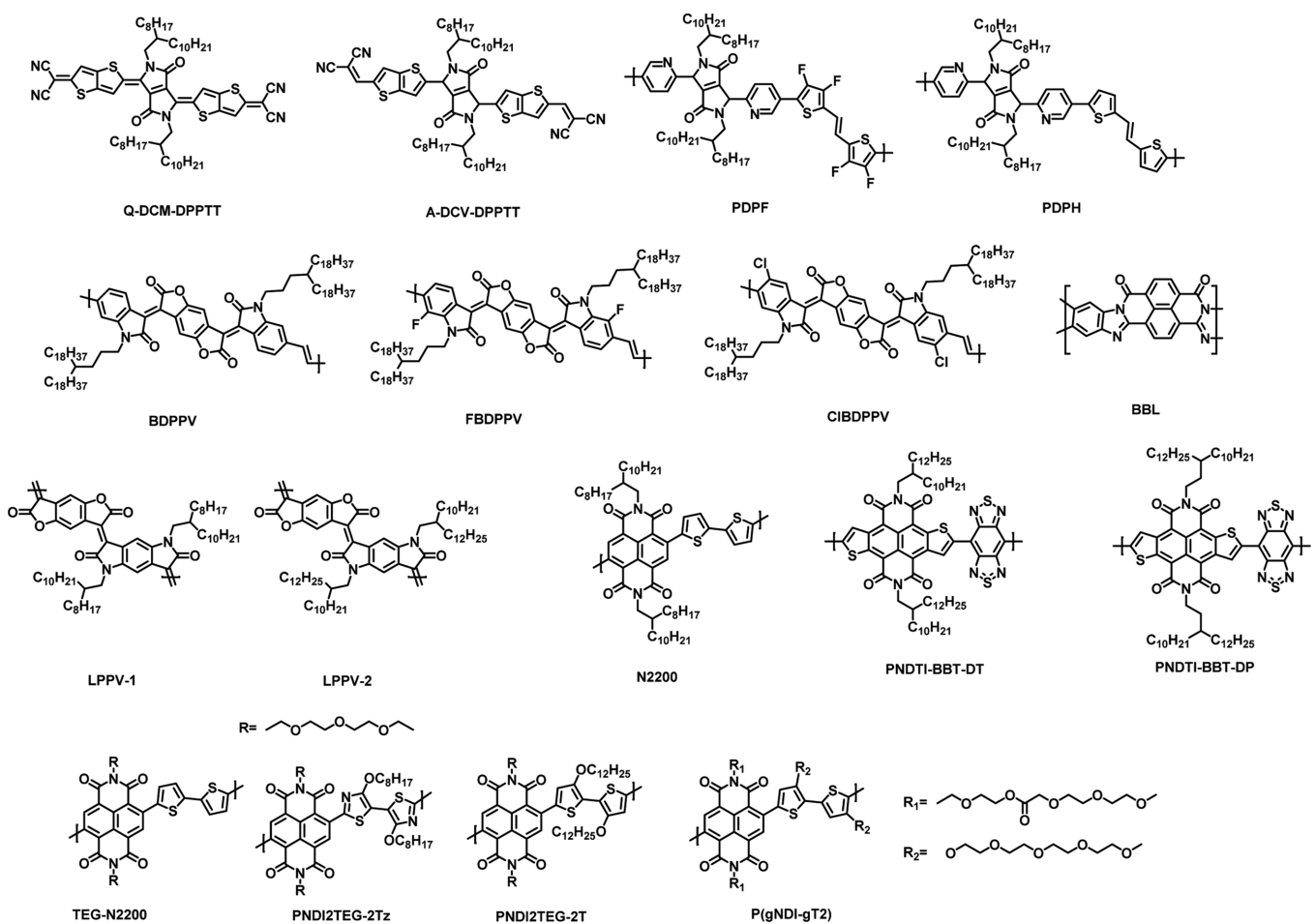
Semiconductor/Dopant	$\sigma_{at\ max\ PF}$ ( $S\ cm^{-1}$ )	$\alpha_{at\ max\ PF}$ ( $\mu V\ K^{-1}$ )	$PF_{max}$ ( $\mu W\ m^{-1}\ K^2$ )	Methods	Ref
Acid-base treated PEDOT:PSS/EMIM-DCA	(1600)	(65)	754	Sequential	16
PEDOT:PSS	(265)	(~400)	23.5	Electrochemical de-doping	19
PEDOT:PSS	930.41	17.99	30.1	DMSO post-treatment	20
PEDOT:PSS	N/A	N/A	38.46	Treated with EMIM-BF <sub>4</sub> /DMSO	20
PEDOT:PSS	~900	~60	~350	EG-immersion	21
PEDOT:PSS	~880 (~980)	~70	469	DMSO-EG immersion	21
PEDOT:PSS	578 (726)	67 (142)	112	Treated with DMSO then DMSO/HZ	22
PEDOT:PSS	1061 (1270)	38.4	157.35	Addition of DMSO and PEO	23
PEDOT:PSS	2170	39.2	334	Treated with H <sub>2</sub> SO <sub>4</sub> /NaOH	24
PEDOT:Tos/TDAE	~67 (300)	~220 (780)	324	Vapor treatment	26
PP-PEDOT:Tos	117 (2120)	930	1270	Electrochemical treatment	17
PEDOT:Tos	(1500)	55 <sup>a</sup>	N/A	PEG-PPG-PEG treatment	27
PBTTT/FTS	1000	33	110	Vapor doping	30
PBTTT/EBSA	1300	14	25	Immersion doping	30
PBTTT/F4TCNQ	220	39	32	Vapor doping-annealed	31
PBTTT/F2TCNQ	36	140	70	Vapor doping-annealed	31
PBTTT/F4TCNQ	670	42	120	Vapor doping-annealed/OTS treated	31
P3HT/TFSI	50	N/A	26	Dipping	32
P3HT/FeCl <sub>3</sub>	254	37.2	35	Wire-bar coating-dipping	33
P3HT/FeCl <sub>3</sub>	45	122	56	Sequential-drop-cast	34
PDPP3T/FeCl <sub>3</sub>	55 (~86)	226	276	Sequential-drop-cast	34
PCDT/FeCl <sub>3</sub>	23 (65)	53 (77)	6.5	Solution mixing	35
PCDTB/FeCl <sub>3</sub>	87 (130)	40	14	Solution mixing	35
PCDTBT/FeCl <sub>3</sub>	160 (500)	34 (70)	19	Solution mixing	35
P3RT/FeCl <sub>3</sub>	17 (50)	75 (124)	12	Dipping	36
P3RSe/FeCl <sub>3</sub>	52	50 (89)	13	Dipping	36
P3RTe/FeCl <sub>3</sub>	46	51 (124)	10	Dipping	36
PDPPS-12/FeCl <sub>3</sub>	(318)	(70)	126	Dipping	37
PDPPSe-12/FeCl <sub>3</sub>	(997)	(70)	300	Dipping	37
PDPPSe-12/FeCl <sub>3</sub>	949 <sup>b</sup>	62.3 <sup>b</sup>	364 <sup>b</sup>	Dipping	37
PCQ/Gav	N/A	>600	>10	Solution mixing	38
pBBTa26-2T/F4TCNQ	43.1	N/A	11.8	Dipping	39
pBBTa26-4T/F4TCNQ	14.1	N/A	1.2	Dipping	39
pBBTa26-TT/F4TCNQ	102.1	N/A	6.8	Dipping	39
PPy/Nap	78.27	5.23	0.21	Solution mixing	40
pBBT-2T-TT/FeCl <sub>3</sub>	232.7 (287)	49.4 (65.4)	65.2	Sequential solution	41
pBBT-2T-2T/FeCl <sub>3</sub>	313.9	(46.6)	43.5	Sequential solution	41
PCDTFBT/F4TCNQ	8.73	213 (946)	31.5	Solution mixing	42
PCDTPT/F4TCNQ	5.13	211 (878)	21.8	Solution mixing	42
PDPP(6-DO) <sub>2</sub> TT/CN6-CP	70	N/A	N/A	Solution mixing	43
p(g <sub>4</sub> 2T-T)/F4TCNQ	100	N/A	N/A	Solution mixing	44
PCPDTSBT/B(C <sub>6</sub> H <sub>5</sub> ) <sub>3</sub>	2.13 (7.47)	190.53 (426.75)	7.73	Solution mixing	45
PCPDTBT/B(C <sub>6</sub> H <sub>5</sub> ) <sub>3</sub>	0.24 (0.65)	427.03 (522.31)	4.41	Solution mixing	45

<sup>a</sup>Value at maximum conductivity. <sup>b</sup>At 55 °C.

ants have been performed during the last few decades, investigations of their n-type counterparts lag far behind owing to their instability toward oxidation, poor charge mobility, limited availability of dopants, and the fact that they are either difficult to process or cannot be processed at ambient atmosphere. The  $\sigma$  of p-type materials has already exceeded 1000 S cm<sup>-1</sup>.<sup>21,26</sup> In contrast, the value of  $\sigma$  of most n-type materials has remained

relatively low and few structures are known to have achieved  $\sigma$  over 1 S cm<sup>-1</sup> after doping.<sup>46</sup> Therefore, in recent times n-type materials and dopants have received more attention, leading to rapid advancements in the development of new n-type TE materials (Figure 2 and Table 2).

A prerequisite for effective n-doping is that the HOMO level of dopants should be higher than the LUMO level of n-type mol-

**Figure 2.** Chemical structures of n-type TE materials.**Table 2.** Summary of TE properties of n-type conjugated molecules. The value in parenthesis is the maximum  $\alpha$  or  $\sigma$ 

Semiconductor/Dopant	$\sigma_{at\ max\ PF}$ ( $S\ cm^{-1}$ )	$\alpha_{at\ max\ PF}$ ( $\mu V\ K^{-1}$ )	$PF_{max}$ ( $\mu W\ m^{-1}\ K^2$ )	Methods	Ref
Q-DCM-DPPTT/N-DMBI	0.11 (0.24 <sup>a</sup> )	-383 (-420 <sup>a</sup> )	1.7 (4.2 <sup>a</sup> )	Solution mixing	15
A-DCV-DPPTT/N-DMBI	0.31 (4.9 <sup>a</sup> )	-568 (-665 <sup>a</sup> )	95 (217 <sup>a</sup> )	Solution mixing	15
N2200/N-DMBI	0.008	-850	0.6	Solution mixing	50
TEG-N2200/N-DMBI	0.17	-153	0.40	Solution mixing	51
p(gNDI-gT2)/N-DMBI	0.3	-190	0.4	Solution mixing	53
P(NDI2TEG-2T)/N-DMBI	$7.0 \times 10^{-4}$	57	$2.3 \times 10^{-4}$	Solution mixing	54
P(NDI2TEG-2Tz)/N-DMBI	1.8	-159	4.5	Solution mixing	54
BBL/TDAE	(1.7)	N/A	0.43	Vapor doping	55
PNNDI-BBT-DP/N-DMBI	5	-169	14.2	Solution mixing	56
PNNDI-BBT-DT/N-DMBI	0.18	-56	0.6	Solution mixing	56
FBDPPV/N-DMBI	14	-210	28	Solution mixing	59
CIBDPPV/N-DMBI	7	-220	16.5	Solution mixing	59
BDPPV/N-DMBI	0.26	-320	1.6	Solution mixing	59
CIBDPPV/TBAF	(0.62)	-99.2	0.63	Solution mixing	60
PDPF/N-DMBI	1.30	-235	4.65	Solution mixing	61
PDPH/N-DMBI	$1.01 \times 10^{-4}$	-87	$5.11 \times 10^{-4}$	Solution mixing	61
PPV-1/N-DMBI	(1.10)	-170	1.96	Solution mixing	63
LPPV-2/N-DMBI	0.07	N/A	0.25	Solution mixing	63

<sup>a</sup>At 373 K.

ecules; therefore, n-type TE materials require a low-lying LUMO.<sup>47</sup> In 2000, Katz *et al.* reported a series of n-alkyl substituted 1,4,5,8-naphthalenetetracarboxylic diimide (NDI) derivatives with high

electron mobility ( $\mu_e$ ) of 0.001–0.1  $cm^2 V^{-1} s^{-1}$  for OTFTs.<sup>48</sup> Later, Facchetti *et al.* synthesized poly[*N,N'*-bis(2-octyldodecyl)-naphthalene-1,4,5,8-bis(dicarboximide)2,6-diyl]-*alt*-5,5'-(2,2'-bithio-

phene) (N2200) exerting high  $\mu_e$  of  $0.45\text{--}0.85\text{ cm}^2\text{ V}^{-1}\text{ s}^{-1}$  in OTFT devices. This discovery focused the attention on NDI-based D-A type TE materials and these structures became one of the most extensively studied n-type TE materials.<sup>49</sup> Subsequent work by Chabinyc *et al.* led them to report the material N2200 and its unusual TE properties in 2014.<sup>50</sup> After doping with 9 mol% of 1,3-dimethyl-2-phenyl-2,3-dihydro-1H-benzo[d]imidazoles (N-DMBI), the optimal  $\sigma$ ,  $\alpha$ , and PF values were determined to be  $-850\text{ }\mu\text{V K}^{-1}$ ,  $8 \times 10^{-3}\text{ S cm}^{-1}$ , and  $0.6\text{ }\mu\text{W m}^{-1}\text{ K}^2$ , respectively. Based on morphological analyses using atomic force microscopy (AFM) and GIWAXS, they observed no significant morphological changes when compared to pristine films. Using the maximum carrier concentration value, they estimated the doping efficiency of  $\sim 1\%$ , indicating that the formation of aggregates on the surface was caused by poor miscibility of the dopant and polymer. The low doping efficiency was the main reason for low PF and the authors suggested that the TE performance of N2200 could be further improved by increasing the miscibility of dopants.

To improve the miscibility of dopants in polymer matrices and the resulting doping efficiency, Koster *et al.* introduced polar triethylene glycol (TEG)-based side-chains instead of nonpolar alkyl chains and synthesized a new polymer TEG-N2200.<sup>51</sup> Using N-DMBI as a dopant, the optimal  $s$ ,  $a$ , and PF were determined to be  $0.17\text{ S cm}^{-1}$ ,  $-153\text{ }\mu\text{V K}^{-1}$ , and  $0.40\text{ }\mu\text{W m}^{-1}\text{ K}^2$ , respectively. They measured the carrier density with admittance spectroscopy and determined the doping efficiency over 10%. The GIWAXS data indicated that TEG-N2200 in neat film had a dominant edge-on orientation in contrast to N2200 (face-on) probably because of different interactions between the polar side-chains and glass substrates. AFM analysis showed that the film morphology had improved substantially, suggesting that the introduction of polar TEG chains improved the miscibility with polar dopants compared to the doped N2200 film. Similarly, Muller *et al.* synthesized a new TE polymer, p(gNDI-gT2) based on NDI-bithiophene units.<sup>52,53</sup> They modified N2200 by incorporating polar oligoethylene glycol (OEG) side-chains on both NDI and the bithiophene moieties. The EPR analysis revealed a doping efficiency of  $\sim 13\%$  at 20 mol% N-DMBI, attributed to the good miscibility of p(gNDI-gT2) and N-DMBI. The increased doping efficiency resulted in a two-fold increase in the conductivity compared to that of the N2200 polymer. The optimal  $\sigma$ ,  $\alpha$ , and PF were  $0.3\text{ S cm}^{-1}$ ,  $-190\text{ }\mu\text{V K}^{-1}$ , and  $0.4\text{ }\mu\text{W m}^{-1}\text{ K}^2$ , respectively.

Koster *et al.* synthesized two kinds of TEG-substituted NDI-based n-type polymers, P(NDI2TEG-2T) and P(NDI2TEG-2Tz). These two polymers differ in that the bithiophene unit in the former was replaced by a bithiazole moiety in the latter. The DFT calculation showed that P(NDI2TEG-2Tz) exhibited a more planar structure compared to P(NDI2TEG-2T) owing to the  $\text{sp}^2\text{-N}$  atoms in the thiazole units. The calculation agreed with the GIWAXS analysis which showed that P(NDI2TEG-2Tz) had the more desirable edge-on orientation. After doping with N-DMBI,  $\sigma$  increased from  $4.8 \times 10^{-11}$  to  $7.0 \times 10^{-4}\text{ S cm}^{-1}$  for P(NDI2TEG-2T) and from  $1.6 \times 10^{-9}$  to  $1.8\text{ S cm}^{-1}$  for P(NDI2TEG-2Tz). The maximum PF values were measured to be  $2.3 \times 10^{-4}$  and  $4.5\text{ }\mu\text{W m}^{-1}\text{ K}^2$  for P(NDI2TEG-2T) and P(NDI2TEG-2Tz), respectively.<sup>54</sup> The result emphasized the importance of chain planarity for efficient charge carrier transport and the resulting electrical/thermoelec-

tric properties. Based on this motivation, Fabiano *et al.* synthesized a ladder-type n-type polymer poly(benzimidazobenzophenanthroline) (BBL) in 2016.<sup>55</sup> The highly fused conjugated backbone without solubilizing side-chains provided a highly rigid and planar polymer backbone with pronounced p-stacking. After doping with the vapor dopant TDAE, the maximum  $\sigma$  of BBL increased from  $\sim 10^{-3}$  to  $1.7\text{ S cm}^{-1}$  and the maximum PF was determined to be  $0.43\text{ }\mu\text{W m}^{-1}\text{ K}^2$ , emphasizing that the chain rigidity and planarity of these ladder-type structures play an important role in improving the  $\sigma$  and PF.

Takimiya *et al.* combined two electron-deficient building blocks, BBT and naphtho[2,3-*b*:6,7-*b*]-dithiophenediimide (NDTI), to synthesize two new polymers P(NDTI-BBT-DP) and P(NDTI-BBT-DT) with different alkyl side-chains, *i.e.*, 3-decylpentadecyl (DP) and 2-decyltetradecyl (DT).<sup>56</sup> Both of these two polymers have low-lying HOMO (-5.5 eV) and LUMO (-4.4 eV) levels. In OTFT devices, the electron mobility  $\mu_e$  of P(NDTI-BBT-DP) was  $0.31\text{ cm}^2\text{ V}^{-1}\text{ s}^{-1}$  and after doping with N-DMBI,  $\sigma$  of  $5\text{ S cm}^{-1}$  and PF of  $14.2\text{ }\mu\text{W m}^{-1}\text{ K}^2$  were obtained. However, P(NDTI-BBT-DT) exhibited  $\mu_e$  of  $0.096\text{ cm}^2\text{ V}^{-1}\text{ s}^{-1}$  in OTFTs and the optimal values of  $\sigma$  and PF ( $0.18\text{ S cm}^{-1}$  and  $0.6\text{ }\mu\text{W m}^{-1}\text{ K}^2$ ) were lower compared to those of P(NDTI-BBT-DP). GIWAXS data showed that the crystallinity of P(NDTI-BBT-DP) film was not affected by doping. They suggested the preserved morphology of P(NDTI-BBT-DP) to be the reason for the higher  $\sigma$  and PF compared to those of P(NDTI-BBT-DT), indicating that a slight modification of the alkyl side-chains can significantly influence the electrical properties.

In 2017, Zhu *et al.* synthesized aromatic-dicyanovinyl-dipyrrolo[3,4-*c*]pyrrole-1,4-diylidene-bis(thieno[3,2-*b*]thiophene) (A-DCV-DPPTT) and quinoid-dicyanomethylene-dipyrrolo[3,4-*c*]pyrrole-1,4-diylidene-bis(thieno[3,2-*b*]thiophene) (Q-DCM-DPPTT) to study the role of a conjugated backbone on the TE properties.<sup>15</sup> A-DCV-DPPTT has a conjugated aromatic backbone whereas Q-DCM-DPPTT has a quinoid structure. A-DCV-DPPTT demonstrated optimal  $\sigma$ ,  $\alpha$ , and PF of  $0.31\text{ S cm}^{-1}$ ,  $-568\text{ }\mu\text{V K}^{-1}$ , and  $95\text{ }\mu\text{W m}^{-1}\text{ K}^2$  respectively, at room temperature. However, when the properties were measured at 373 K, the PF increased to  $217\text{ }\mu\text{W m}^{-1}\text{ K}^2$ , which is the highest PF for n-type TE molecules among those reported thus far. In contrast, Q-DCM-DPPTT exhibited much lower  $\sigma$ ,  $\alpha$ , and PF of  $0.11\text{ S cm}^{-1}$ ,  $-383\text{ }\mu\text{V K}^{-1}$ , and  $1.7\text{ }\mu\text{W m}^{-1}\text{ K}^2$ , respectively, and the PF measured at 373 K was  $4.2\text{ }\mu\text{W m}^{-1}\text{ K}^2$ . After doping with N-DMBI, A-DCV-DPPTT films underwent no obvious changes in their morphology even at a dopant concentration of approximately 10 wt%. In the case of the Q-DCM-DPPTT films, the dopants started to aggregate on the film as the dopant concentration was increased (5 wt% N-DMBI). GIWAXS measurements of A-DCV-DPPTT revealed no significant changes and displayed stronger edge-on scattering peaks compared to Q-DCM-DPPTT. They suggested that the large difference in the TE properties was caused by the different degree of conjugation of the backbone, which resulted in the morphology and doping efficiency being different.

Recently, Pei *et al.* reported a series of promising n-type TE polymers based on different conjugated backbones. For example, in 2015, they synthesized an n-type polymer based on the benzodifuranone-phenylenevinylene moiety (BDPPV), which has a partially locked (two-thirds of the backbone) conformation

that fortifies its planarity.<sup>57,58</sup> The electron mobility  $\mu_e$  of this polymer reached a maximum of  $1.1 \text{ cm}^2 \text{ V}^{-1} \text{ s}^{-1}$ . They additionally synthesized a fluorine-substituted polymer, FBDPPV, where the F-substitution not only lowered the LUMO, but also fully locked the chain conformation *via* the formation of intramolecular hydrogen bonds, thereby increasing  $\mu_e$  up to  $1.70 \text{ cm}^2 \text{ V}^{-1} \text{ s}^{-1}$  in ambient atmosphere. The equivalent polymer with chlorine substituents, CIBDPPV, was also prepared, enabling researchers to explore the TE properties and the effects of the halogen atoms on the TE properties of BDPPV polymers.<sup>59</sup> FBDPPV doped with N-DMBI showed impressively high  $\sigma$  of  $14 \text{ S cm}^{-1}$  and PF of  $28 \mu\text{W m}^{-1} \text{ K}^2$ , when compared with the other two polymers ( $\sigma = 0.26$  and  $7 \text{ S cm}^{-1}$ ; PF =  $1.6$  and  $16.5 \mu\text{W m}^{-1} \text{ K}^2$  for BDPPV and CIBDPPV, respectively). AFM analysis indicated that all three films had remarkably smooth surfaces (root mean square roughness  $\sim 0.60 \text{ nm}$ ) at 5 wt% N-DMBI, and the morphology did not significantly change even at 10 wt% dopant. This good miscibility of the dopants in the case of all three of the films was suggested to be caused by the low crystallinity of the three films; in fact, GIWAXS analysis revealed low lamellar diffraction peaks. The low crystallinity of the BDPPV derivatives was also considered to allow improved dispersion of the dopants in the polymer films to increase the doping efficiency. In 2017, Katz *et al.* also reported that CIBDPPV doped with tetrabutylammonium fluoride (TBAF) was stable under ambient conditions. Doping with 25 mol% TBAF enabled them to achieve the maximum  $\sigma$  of  $0.62 \text{ S cm}^{-1}$  and PF of  $0.63 \mu\text{W m}^{-1} \text{ K}^2$  in air. The good stability was maintained even after the doped compound was exposed to air for a week (maintaining  $\sigma = 0.1 \text{ S cm}^{-1}$ ).<sup>60</sup>

In addition, two different DPP-based D-A polymers, poly[2,5-bis(2-octyldodecyl)-3,6-di(pyridin-2-yl)-pyrrolo[3,4-c]pyrrole-1,4(2H,5H)-dionealt-(E)-2,2'-(ethene-1,2-diylbis(thiophene-5,2-diyl))]] (PDPH) and poly[2,5-bis(2-octyldodecyl)-3,6-di(pyridin-2-yl)-pyrrolo[3,4-c]pyrrole-1,4(2H,5H)-dionealt-(E)-2,2'-(ethene-1,2-diylbis(3,4-difluorothiophene-5,2-diyl))]] (PDPF) with fluorine substituents were synthesized.<sup>61</sup> Although their neat films exhibited similar  $\mu_e$  values ( $1.34$  and  $1.19 \text{ cm}^2 \text{ V}^{-1} \text{ s}^{-1}$  for PDPH and PDPF, respectively), the  $\sigma$  and PF values significantly differed after doping with N-DMBI. After doping, PDPF had optimal  $\sigma$  and PF values of  $1.30 \text{ S cm}^{-1}$  and  $4.65 \mu\text{W m}^{-1} \text{ K}^2$  and those of PDPH were  $1.01 \times 10^{-4} \text{ S cm}^{-1}$  and  $5.11 \times 10^{-4} \mu\text{W m}^{-1} \text{ K}^2$ , respectively. Morphological study using GIWAXS showed that both PDPH and PDPF had strong edge-on orientation. As the dopant concentration increased, the film morphology of PDPH was disturbed and N-DMBI aggregates appeared. On the other hand, PDPF exhibited uniform morphology with a higher doping efficiency, suggesting that simple modification by introducing F substitution had the effect of locking the conformation, which lowered both the HOMO and LUMO, resulting in enhanced doping efficiency and TE properties. In 2019, a new n-dopant (N-DMBI)<sub>2</sub>, which is a dimeric structure of N-DMBI, was designed and synthesized by considering the high reduction ability (similar to that of the dimeric metal dopant (RuCp\*mes)<sub>2</sub>) and size of the resulting dopant counterion after doping occurs.<sup>62</sup> Pei and coworkers studied the effects of the dopant on the TE properties of FBDPPV by utilizing three different dopants of (N-DMBI)<sub>2</sub>, N-DMBI, and (RuCp\*mes)<sub>2</sub>. The maximum  $\sigma$  of FBDPPV with N-DMBI

and (N-DMBI)<sub>2</sub> was  $\sim 8 \text{ S cm}^{-1}$ , but  $\sigma$  with (RuCp\*mes)<sub>2</sub> was  $1.6 \text{ S cm}^{-1}$ . Even though N-DMBI and (N-DMBI)<sub>2</sub> dopants yielded similar  $\sigma$ , 43 mol% of N-DMBI was used whereas only 10.7 mol% of (N-DMBI)<sub>2</sub> was used to reach the maximum  $\sigma$ , indicating the higher doping efficiency of (N-DMBI)<sub>2</sub>. The PF values were determined to be approximately 7, 5, and  $1 \mu\text{W m}^{-1} \text{ K}^2$  with (N-DMBI)<sub>2</sub>, N-DMBI, and (RuCp\*mes)<sub>2</sub> as dopants, respectively. Morphological analyses by AFM, GIWAXS, and scanning kelvin probe microscopy (SKPM) indicated that (N-DMBI)<sub>2</sub> demonstrated less perturbation of the original ordered microstructures because of its smaller and more planar counterion N-DMBI<sup>+</sup> relative to the bulky RuCp\*mes<sup>+</sup>. The researchers claimed that not only the doping mechanism but also the shape (or size) of dopant counterions strongly influenced the TE and charge transport properties. To further investigate the effect of backbone rigidity, Pei *et al.* synthesized poly{(2,6-dioxo-6,7-dihydrobenzo[1,2-*b*:4,5-*b*']difuran-3(2*H*)-ylidene)-1,5-bis(2-octyldodecyl)-5,7-dihydropyrrolo[2,3-*f*]indole-2,6(1*H*,3*H*)-dione} (LPPV-1) and poly{(2,6-dioxo-6,7-dihydrobenzo[1,2-*b*:4,5-*b*']difuran-3(2*H*)-ylidene)-1,5-bis(2-decytetradecyl)-5,7-dihydropyrrolo[2,3-*f*]indole-2,6(1*H*,3*H*)-dione} (LPPV-2) with various alkyl side-chains.<sup>63</sup> These two polymers differ in that LPPV-1 contains shorter octyldodecyl side-chains, whereas LPPV-2 has longer decyltetradecyl side-chains. Both of these polymers also have a locked conformation with structures that are nearly torsion-free. Further, the small changes in the crystallinity of both polymers (LPPV-1 and LPPV-2) upon doping with N-DMBI indicated that the dopants were well mixed in the amorphous regions. LPPV-1 showed the higher  $\sigma$  ( $1.1 \text{ S cm}^{-1}$ ) and PF ( $1.96 \mu\text{W m}^{-1} \text{ K}^2$ ) than LPPV-2 ( $\sigma = 0.07 \text{ S cm}^{-1}$  and PF =  $0.25 \mu\text{W m}^{-1} \text{ K}^2$ ) with high stability when exposed to air (PF only decreased by 2% after exposure to air for 7 days). The strong planarity of the conjugated backbone combined with strong side-chain interaction as a result of the shorter alkyl side-chain was suggested to reduce the conformational disorder of LPPV-1 and to elongate its polaron delocalization.

### 3. Molecular Doping

Molecular doping is a powerful technique to tune the  $\sigma$  of organic materials as the doping process introduces additional charge carriers (*i.e.*, polarons and bipolarons) into the molecular backbone *via* charge transfer (chemical oxidation or reduction).<sup>13,20,64-66</sup> Several p- and n-type dopants have been developed and their molecular structures are collected in Figure 3. In particular, p-doping requires the HOMO level of a polymer (known as an electron-rich p-type polymer) to be close to or higher than the LUMO level of the dopant to enable positive polarons (and/or bipolarons) to be introduced into the polymer chain *via* efficient electron transfer from the polymer to the dopant.<sup>46</sup> Coprocessing of the polymer and dopant is the most common way of doping. As an example of p-doping, Muller *et al.* explored the coprocessing of p(g<sub>4</sub>T-T) and the dopant F4TCNQ in a 1:1 mixture of acetonitrile and chloroform to dope the polymer.<sup>44</sup> Upon doping, the increased carrier density not only increased the  $\sigma$  but also bleached the absorption of the neutral polymer at 600 nm as shown in the UV-vis spectra of p(g<sub>4</sub>T-T) film (Figure 4). The absorption of ionized F4TCNQ at 410 and 700 nm as well as

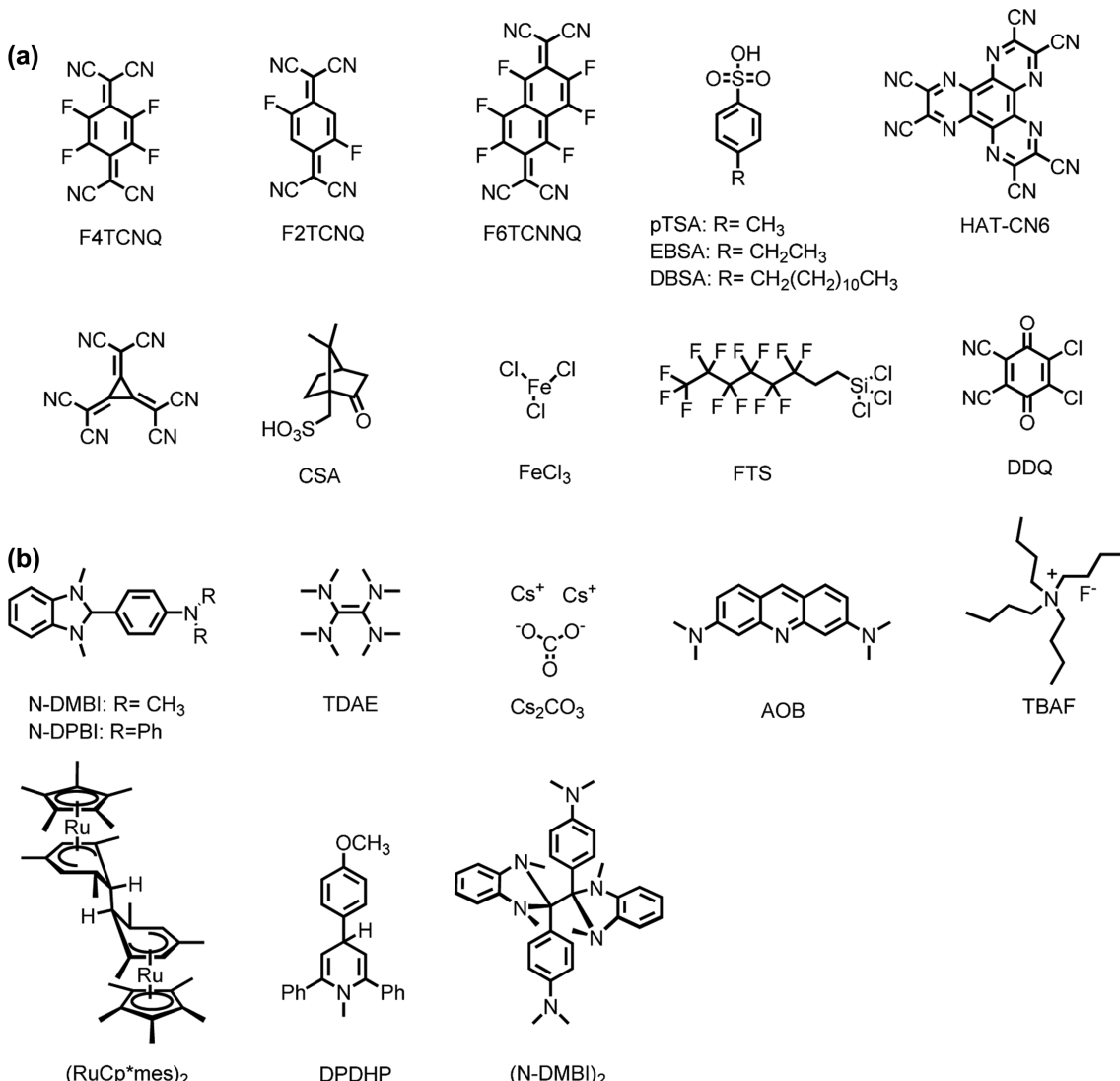


**Figure 3.** Chemical structures of (a) p- and (b) n-type dopants.

that of the polarons in the polymer backbone above 700 nm were gradually enhanced with increasing [F4TCNQ] = 0–20 mol%. The neutral F4TCNQ absorption at 390 nm also increased as the dopant concentration increased. In the case of n-doping, the dopants transfer electrons to the LUMO of electron-deficient n-type polymers, generating negative polarons (and/or bipolarons) along the polymer backbone. As an example, the most widely used n-type dopant, N-DMBI, can dope polymers *via* hydrogen atom transfer followed by the creation of an electron transfer pathway (Figure 4). After casting the films of a mixture of the polymer and dopant, the films are heated to form N-DMBI neutral radicals. This neutral radical has an exceptionally high singly occupied molecular orbital (SOMO) level, allowing an electron to be instantly transferred to the LUMO of the polymer, leading to the formation of a stable N-DMBI cation.<sup>67</sup> Therefore, the polymer is reduced by electron transfer to generate negative polarons and bipolarons in the polymer backbone.

The method according to which a dopant is introduced into a polymer plays a critical role in determining the doping efficacy by charge transfer. “Solution-mixed doping” in which the doped polymer film is fabricated by casting a solution containing a

mixture of the polymer and the dopant in the desired ratio, is the most commonly used method owing to its simplicity.<sup>31,68–70</sup> However, the use of this method for doping often results in the formation of aggregates when the dopant concentration is increased. Charge transfer between the polymer and dopant forms a charge transfer (CT) complex and the fact that the solubility of the charged species differs from that of the neutral polymers (and dopants), causes them to readily precipitate from the organic solvents used for processing to ultimately yield poor-quality films.<sup>70,71</sup> In addition, aggregation also occurs owing to the presence of excess dopants, which in turn affects the morphology of films with significant phase separation.<sup>72</sup> Therefore, casted films fabricated by solution-mixed doping with high dopant concentrations often lead to blended film morphologies that exhibit low carrier mobilities.<sup>73</sup> To circumvent these problems, the one-step solution-mixing process could be replaced by a two-step process of “sequential doping.” First, the pristine polymer solution is pre-casted, after which it is exposed to dopants in a secondary step. Exposure of the pre-casted films to dopants is often accomplished by immersion, solution casting (drop casting or spin coating), and vapor doping. In sequential doping *via* immersion and solu-

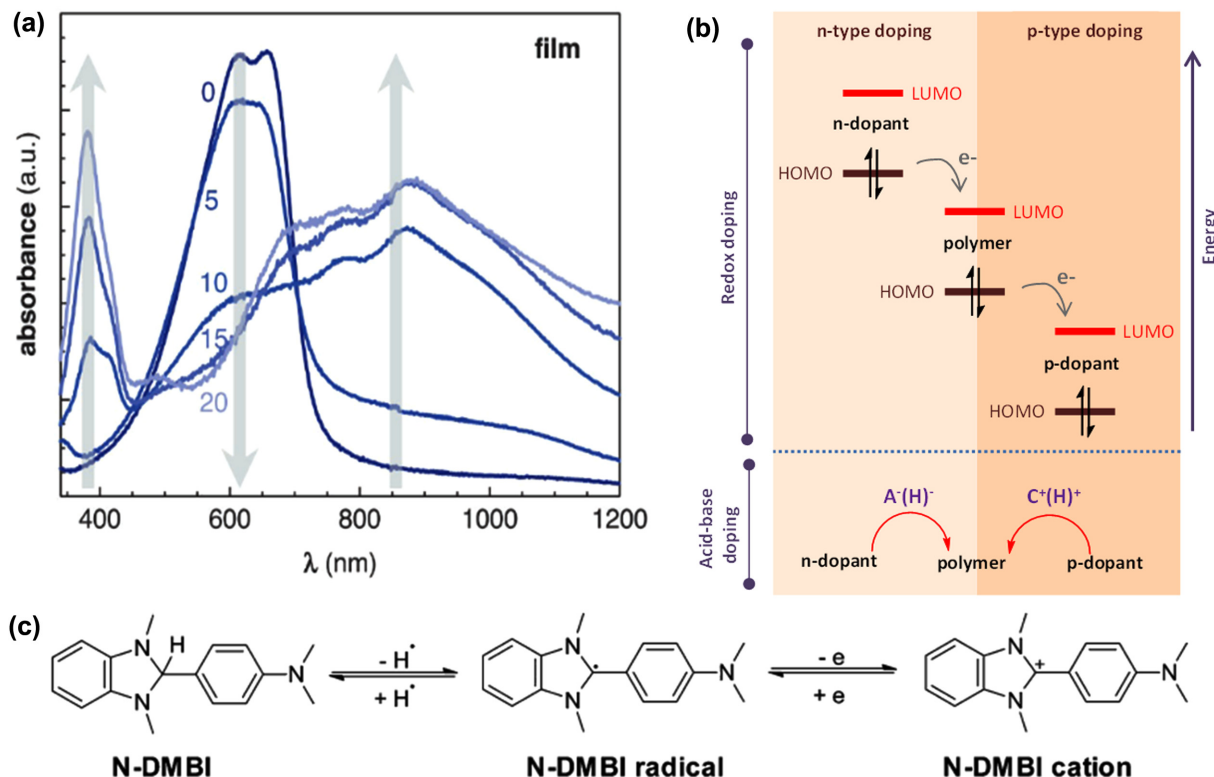


**Figure 4.** (a) Spectral changes in UV-Vis spectra of p(g,2T-T) doped with 5, 10, 15, and 20 mol% F4TCNQ. Reproduced with permission from Ref. 44, C. Muller *et al.*, *Adv. Mater.*, **29**, 1700930 (2017). © 2017, John Wiley and Sons. (b) Basic principle of acid-base doping and energy level diagram of redox doping. (c) Proposed mechanism of hydrogen and electron transfer for n-doping by N-DMBI.

tion-casting, selection of a suitable solvent for the dopants is imperative. That is, dopants should be dissolved in a semi-orthogonal solvent in which the pre-cast polymer films should not dissolve; rather, the films should expand to enable the dopants to penetrate the film without disturbing the ordered polymer packing.<sup>74</sup> The doping level can be adjusted by changing the dopant concentration and the expandability of the film by using different solvents in the second step in which the dopant solution is cast.<sup>75</sup> Although this fabrication method is not as simple as the conventional solution-mixed doping process, it offers several advantages such as the preserved morphology of pre-cast films, smooth film morphology, and higher charge mobility and  $\sigma$  with fewer trapped charge carriers.<sup>74,76</sup>

Many research groups implemented sequential doping methods in several different ways. The commonly used method that has emerged is the “vapor doping method” or “solid state diffusion”, which is a sequential-doping method because the dopant is introduced onto pre-cast polymer films; hence, the method could be also referred to as “vapor sequential doping”. Dopant vapor is deposited onto the pre-casted film by heating the dopants (sublimation or evaporation) to allow the dopant molecules to penetrate the polymer chains. Many recent reports describe the doping of P3HT and PBTETT by F4TCNQ with the aim of comparing the solution-mixed doping and vapor doping methods. These studies proved that the higher  $\sigma$  resulting from the vapor doping method is attributable to the crystalline ordering of the films after doping, because the morphology of the films was not disrupted, whereas the solution-mixed doping method produced considerably rougher films even at much lower doping levels

(less than 1 mol% in the P3HT:F4TCNQ system dissolved in chlorobenzene).<sup>30,31,76-78</sup> One of the main demerits of sequential doping methods is that they can only be used for thin films (<100 nm) because dopant penetration into a solid film is limited.<sup>79</sup> However, recently Fontana *et al.* demonstrated successfully that even ~2-μm-thick films can be efficiently doped by solution sequential doping by using an appropriate choice of solvent and dopant concentration.<sup>74</sup> These thick films were prepared by drop casting P3HT solution dissolved in o-dichlorobenzene onto glass substrates, which were then slowly dried by placing them inside a covered Petri dish for 2 days. Once the polymer layer had dried, the dopant solution (F4TCNQ in dichloromethane) was spin casted to form a layer on top of the polymer. The thickest film (2 μm) showed the highest  $\sigma$  of approximately 5 S cm<sup>-1</sup> owing to the higher ordering of polymers, which increases the carrier mobility.

In addition, as the doped carrier concentration increases,  $\sigma$  increases, but  $\alpha$  decreases, showing an inverse relationship. Zhu *et al.* reported the solution-mixed doping of n-type polymers, A-DCV-DPPTT and Q-DCM-DPPTT with N-DMBI. The undoped A-DCV-DPPTT and Q-DCM-DPPTT films showed high  $\alpha$  values of -1215 and -875  $\mu$ V K<sup>-1</sup>, respectively. However, the  $\sigma$  for both pristine films were lower than 0.001 S cm<sup>-1</sup>. Upon doping with N-DMBI, the  $\alpha$  of A-DCV-DPPTT decreased to -830  $\mu$ V K<sup>-1</sup> at 1 wt% N-DMBI and -568  $\mu$ V K<sup>-1</sup> at 5 wt% N-DMBI, while the  $\sigma$  increased to 0.3 and 3.1 S cm<sup>-1</sup>, respectively. The doped Q-DCM-DPPTT also showed a similar inverse trend: as  $\alpha$  decreased from -875 to -383  $\mu$ V K<sup>-1</sup>, the  $\sigma$  increased up to ~0.1 S cm<sup>-1</sup> at 5 wt% N-DMBI.<sup>15</sup> Woo *et al.* reported a p-type polymer PCPDTTSBT showing the

maximum  $\sigma$  of  $7.47 \text{ S cm}^{-1}$  at 29 mol% of  $\text{B}(\text{C}_6\text{F}_5)_3$  dopants. By varying  $[\text{B}(\text{C}_6\text{F}_5)_3]$  from 3 to 34 mol%, the  $\alpha$  values decreased from 426.75 to  $60.19 \mu\text{V K}^{-1}$ , and they obtained the maximum PF of  $7.73 \mu\text{W m}^{-1}\text{K}^2$  with  $\sigma = 2.13 \text{ S cm}^{-1}$  and  $\alpha = 190.53 \mu\text{V K}^{-1}$  at 9 mol% of dopant.<sup>45</sup> Thus, it is necessary to precisely control the doping concentration to adjust the  $\sigma$  and  $\alpha$  values to obtain the maximum PF. Decoupling the trade-off relationship of  $\sigma$  and  $\alpha$  needs to be investigated for further improvement of the PF.

#### 4. Charge Transport Models

Despite extensive studies on organic TE materials and devices that led to remarkable improvements in the TE performance, their charge transport behavior is not yet clearly understood. A standard and robust model to describe the charge carrier transport behavior in disordered organic materials has yet to be proposed because of the many localized charge carriers and complex microstructures, which make it difficult to define the carrier density ( $n$ ) and mobility ( $\mu$ ) in organic TE devices.<sup>80</sup> Recently, several efforts have been made to understand the charge transport behavior in organic TE devices by studying the relation between  $\alpha$  and  $\sigma$ .

##### 4.1. Mott mobility edge model and variable range hopping model

In the Mott mobility edge (ME) model, ME is the highest energy level that separates localized and non-localized states in the conduction band (or valence band) of non-crystalline materials.<sup>81</sup> This model assumes that the carriers below ME are trapped and thus do not contribute to the conduction, whereas the carriers above the ME are delocalized and freely conduct electricity similar to a metal. According to the ME model, the  $\sigma$  and  $\alpha$  of the amorphous semiconductors can be expressed by the following equations:

$$\sigma = \sigma_0 \exp \left\{ -\frac{E_c - E_F}{k_B T} \right\} \quad (2)$$

$$\alpha = \frac{k_B}{e} \left( \frac{E_F - E_V}{k_B T} + A \right) \quad (3)$$

Here,  $\sigma_0$  is the pre-exponential factor,  $E_c$  is the mobility edge,  $k_B$  is Boltzmann's constant,  $e$  is the unit charge,  $T$  is the temperature,  $A$  is dimensionless and greater than 1 and is related to the weighted conductivity DOS,  $E_F$  is the Fermi energy, and  $E_V$  is the valence energy.<sup>82-84</sup> Chabiny *et al.* used an estimation of the activation energy  $E_A$  as being correlated to  $E_F - E_V$  and the experimental trends of  $E_A \propto \ln \sigma$  to derive the relationship between  $\alpha$  and  $\sigma$  by using the following equation:<sup>82</sup>

$$\alpha = \frac{k_B}{e} \left( \frac{B \ln \sigma + C}{k_B T} \right) + A \quad (4)$$

where  $B$  and  $C$  are constants and are given by fitting the activation energy to the conductivity. The solid line in Figure 5 shows the  $\alpha-\sigma$  fitting curve based on this equation. However, the model does not fit the experimental data well. This could be explained

by considering that the assumptions of the model may not be appropriate for the nature of the organic (or polymeric) semiconductors. First, Mott established this model for disordered semiconductors with homogeneity; however, contrary to the assumption of the model, the  $\sigma$  of polymeric semiconductors is thermally activated even for carriers with energy above the transport edge.

Another well-known charge transport model for explaining amorphous inorganic semiconductors and organic materials is the hopping transport model.<sup>85,86</sup> Owing to their energetic and structural disorder, these materials form localized states among which charge transport occurs *via* thermally assisted hopping. Two types of hopping conduction models have been reported: nearest neighbor hopping (NNH) and variable range hopping (VRH). The probability of hopping between two states that are separated in terms of both their spatial locations and their energies is generally given by the Millar-Abrahams transition rate.<sup>87</sup> When charge carriers have sufficient energy, spatial separation becomes the dominant factor; thus, they hop to the nearest empty neighboring site (NNH model). However, at low thermal energies, charge carriers become energetically favorable to tunnel to non-nearest sites with lower energies irrespective of their spatial separation and this is referred to as VRH. The VRH model assumes that charge transport occurs only around the  $E_F$  and at a constant DOS. The  $\sigma$  and  $\alpha$  can be described as follows:<sup>84</sup>

$$\sigma = \sigma_0 \exp \left\{ -\left( \frac{T_0}{T} \right)^{\frac{1}{1+d}} \right\} \quad (5)$$

$$\alpha = \frac{k_B^2}{e} (T_0 T)^{\frac{1}{2}} \frac{d \ln N}{d E} \Big|_{E_F} \quad (6)$$

where  $\sigma_0$  is the pre-exponential factor,  $T$  is temperature, the variable  $T_0$  is found *via* the temperature dependent  $\sigma$  of the Mott relation, and  $N$  is the DOS. In 2015, Chabiny *et al.* also tried to fit a curve to the  $\alpha-\sigma$  relationship based on the VRH model (dash-single dotted line in Figure 5). However, it also did not fit the experimental data of organic semiconductors because the estimated value of  $\alpha$  was too small (of the order of  $10 \mu\text{V K}^{-1}$ ), whereas the  $\alpha$  of semiconducting polymers normally has an exceedingly higher value in all conductivity ranges.

##### 4.2. Power law relation

As shown above, it is difficult to explain the relationship between  $\alpha$  and  $\sigma$  of semiconducting (or conducting) polymers with pre-established models. In 2015, Chabiny *et al.* discovered a trend that shows a surprisingly good fit over a wide range of conductivities in which the thermopower curve is fit to the empirical power law following the equation below:

$$\alpha = \frac{k_B}{e} \left( \frac{\sigma}{\sigma_\alpha} \right)^{-1/4} \quad (7)$$

where  $\sigma_\alpha$  is an unknown conductivity constant that is independent of the carrier concentration. Consequently, the PF is related to the inverse square-root of the conductivity,  $\text{PF} \propto \sigma^{-1/2}$  (dotted line in Figure 5(a) and Figure 5(b)).<sup>82</sup> Here, they measured and plotted the thermoelectric properties of the well-known poly-

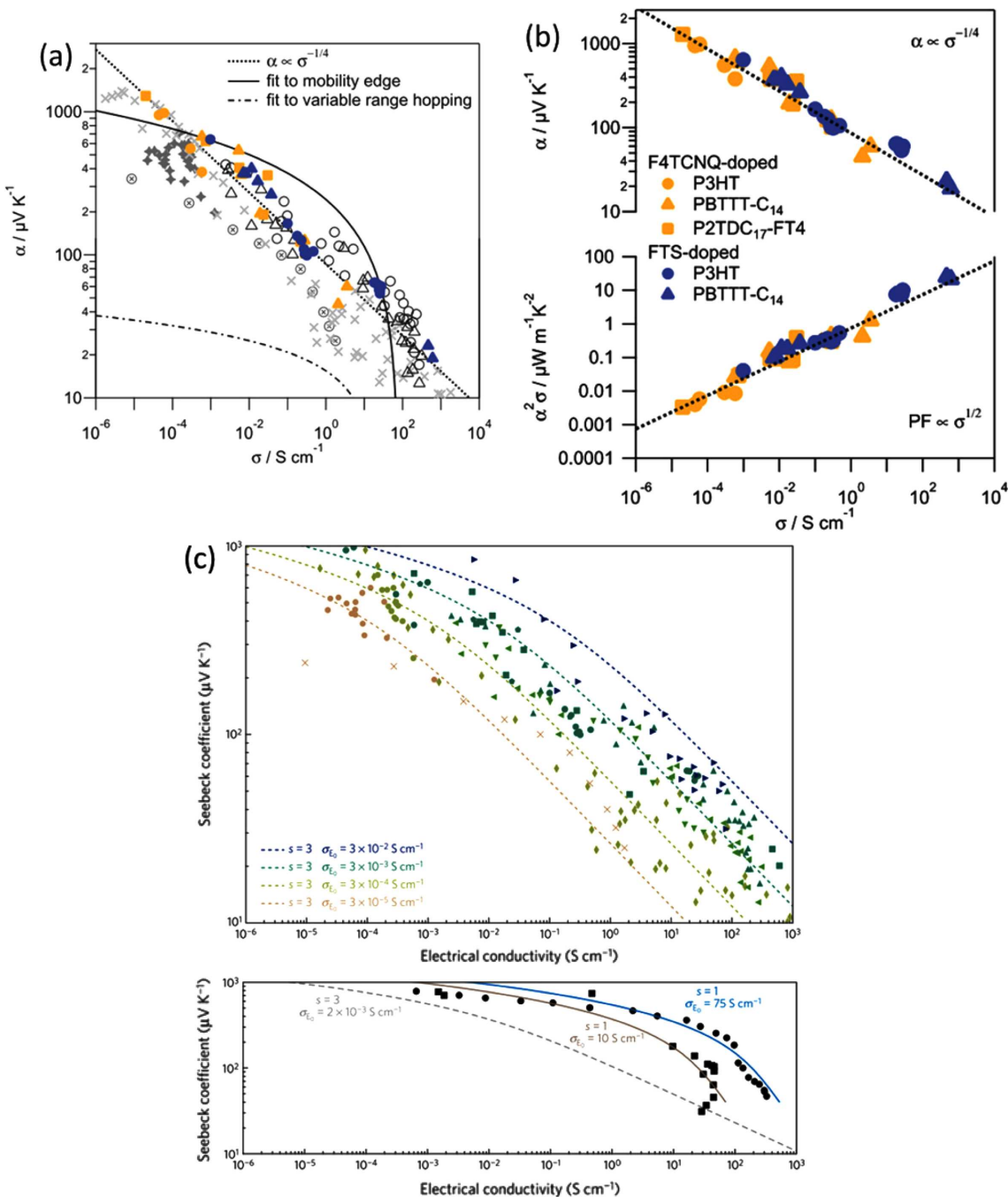


**Figure 5.** (a) Seebeck coefficient as a function of electrical conductivity. An empirical power law (dotted line), mobility edge model (solid line), and variable range hopping model (dash-single dotted line). (b) Thermopower (top) and PF (bottom) as a function of electrical conductivity. The dashed lines indicate an empirical fit of  $\alpha$  proportional to  $\sigma^{1/4}$  and PF proportional to  $\sigma^{1/2}$ . Reproduced with permission from Ref. 82, A. M. Glaudell *et al.*, *Adv. Energy Mater.*, **5**, 1401072 (2015). © 2015, John Wiley and Sons. (c)  $\alpha$ - $\sigma$  relation fitted by Kang-Snyder model. Reproduced with permission from Ref. 80, S. D. Kang and G. J. Snyder, *Nat. Mater.*, **16**, 252 (2017). © 2016, Springer Nature.

thiophene-based polymers, P3HT, PBTTT-C<sub>14</sub>, P2TDC<sub>17</sub>-FT4<sup>88-91</sup> doped with F4TCNQ, and FTS and found that all of them show a clear trend that fits the empirical power law with the parameter  $\sigma_\alpha \sim 1 \text{ S cm}^{-1}$  (plotted symbols in Figure 5(b)). Because of its simplicity of application, many researchers explored the  $\alpha$ - $\sigma$  relation and many polymeric systems were found to be in good agreement with the empirical model. For example, in 2017, Katz *et al.* reported that the  $\alpha$ - $\sigma$  relation of doped polythiophene-based polymers (PQT12, PQTS12, PDTDE12, and PDTDES12) fitted this model well especially in high  $\sigma$  ranges.<sup>92</sup> The blended polymers

PBTTTC12 and PBTTTSC12 were also shown to follow the power law relationship.<sup>93</sup> In addition, Kemerink *et al.* found similar empirical thermopower behavior for the well-known n-type material, PCBM, doped with 4-(1,3-dimethyl-2,3-dihydro-1*H*-benzoimidazol-2-yl)-*N,N*-diphenylaniline (N-DPBI).<sup>94</sup>

#### 4.3. Kang - Snyder model

Although the empirical power law developed by Chabiny *et al.* seems to fit several polymers with various dopants and doping

methods as discussed above, their physical origin and meanings are not clear, thereby limiting the application of this power law. In 2017, Kang and Snyder suggested a new empirical model (the K-S model) which suggested a more profound understanding of the charge transport properties of organic TE systems.<sup>80</sup> They defined the transport function  $\sigma_E(E)$  using two essential parameters, the transport edge  $E_t$  and transport parameter  $\sigma$ :

$$\begin{aligned}\sigma_E(E, T) &= \sigma_{E0}(T) \times \left( \frac{E - E_t}{k_B T} \right)^s \quad (E > E_t) \\ &= 0 \quad (E < E_t)\end{aligned}\quad (8)$$

Here,  $\sigma_{E0}(T)$  is the transport coefficient, which is a temperature-dependent but energy independent parameter,  $k_B$  is Boltzmann's constant, and  $T$  is the temperature. The definitions of  $\sigma$  and  $\alpha$  were obtained in terms of  $\sigma$  and  $\eta$  by applying this equation to the generalized Boltzmann transport equations:

$$\sigma = \sigma_{E0}(T) \times sF_{s-1}(\eta) \quad (9)$$

$$\alpha = \frac{k_B}{q} \left[ \frac{(s+1)F_s(\eta)}{sF_{s-1}(\eta)} - \eta \right] \quad (10)$$

where  $F_s$  is the Fermi-Dirac integral,  $\eta = (E_F - E)/k_B T$  is the reduced chemical potential, and  $q$  is the unit charge. The transport coefficient  $\sigma_{E0}(T)$  acts as a weighted mobility, which determines the magnitude of  $\sigma$ . The transport parameter  $s$  indicates the energy dependency of the charge transport. By fitting the  $\alpha$ - $\sigma$  relation of organic TE systems by the K-S model, it is possible to obtain information on their charge transport properties. In Mott's mobility edge model, charge carriers are transported similarly to free electrons above the transport edge, *i.e.*, transport is energy independent with  $s = 0$ . The  $\alpha$ - $\sigma$  relations of various semiconducting polymers (such as P3HT, PBTTC-C<sub>14</sub>, and P2TDC<sub>17</sub>-FT4) provided a surprisingly good fit with  $s = 3$  (Figure 5), indicating that charge transport above  $E_t$  has a strong energy dependence due to the ionized-impurity scattering. To date, only a few PEDOT-based systems (PEDOT:Tos<sup>26</sup> and PEDOS-C<sub>6</sub><sup>95</sup>) have been reported to follow the  $\alpha$ - $\sigma$  curve with  $s = 1$  ( $\sigma_{E0} = 75$  and  $10 \text{ S cm}^{-1}$ , respectively) among the organic TE materials reported thus far, demonstrating atypical charge transport properties (depending on acoustic-phonon scatterings) with high thermoelectric properties compared to other semiconducting polymers. Therefore, a strong demand has arisen to develop new organic TE systems with  $s = 1$  with a high  $\sigma_{E0}$  value to achieve high TE properties for which ZT exceeds 1.

Several recent studies analyzed the charge transport properties on the basis of the K-S model. Gleason *et al.* compared the carrier mobilities of PEDOT thin films fabricated by oxidative chemical vapor deposition.<sup>96</sup> They compared the transport coefficient,  $\sigma_{E0}$ , of PEDOT films with different orientations and different deposition temperatures. They also calculated and compared the  $W_\gamma$  of PEDOT films, which is the energy barrier for inter-crystallite percolation carrier transport, by using the equation  $\sigma_{E0} \propto \exp\left[-\left(\frac{W_\gamma}{k_B T}\right)^\gamma\right]$ , where  $\gamma$  is the dimensionality factor. Their analyses with the values of  $\sigma_{E0}$  and  $W_\gamma$  indicated that the films with face-on orientation and deposited at high temperature had superior transport properties compared to the films with edge-on orientation. In addition, in the original report of Kang

and Snyder, the factors responsible for determining the transport parameter,  $\sigma$ , were unclear. Recently, Venkataraman *et al.* showed that the spatial distribution of dopants in the doped polymer films can profoundly affect the  $\alpha$ - $\sigma$  relation because it significantly influences the degree of energetic disorder and changes the DOS.<sup>97</sup> They suggested that homogeneous doping reduced the energetic disorder (with  $s = 1$ ) and improved charge transport and thermoelectric performance.

## 5. Flexible thermoelectric devices based on organic thermoelectric materials

TE devices based on organic materials have been of vital interest for wearable applications because they are lightweight, have low thermal conductivity, portability, and breathability, and are easily attached to clothes and curved surfaces. Flexible TE devices have been fabricated with integration into flexible substrates including fabrics,<sup>98,99</sup> organic elastomers such as polydimethylsiloxane (PDMS),<sup>100,101</sup> polyethylene terephthalate (PET),<sup>9,102-104</sup> polyurethane (PU),<sup>105</sup> and polyimide<sup>106-108</sup> by using diverse methods such as printing,<sup>102</sup> vacuum filtration,<sup>109</sup> e-spraying,<sup>105</sup> solvent evaporation<sup>101</sup> and wet spinning.<sup>110</sup> The integration of wearable TE devices into textile-based clothing has been attempted; however, their TE performance needs to be balanced with the aesthetics and comfort of the clothing. Additionally, the maximum output power of polymer-based-organic TE generators had reported to be too low (< 1  $\mu\text{W}$ ) for practical application.<sup>111</sup> Many research groups aiming to solve the low energy harvesting efficiency have attempted to enhance the properties of organic TE generators by chemical processing<sup>107</sup> or by hybridization with highly conductive materials such as inorganic<sup>9,104</sup> and carbon-based materials.<sup>110,112</sup> In addition, research to lower the internal resistance of TE modules<sup>100,103</sup> and to improve the structural efficiency to maintain the temperature difference between the hot and cold sides was conducted for enhanced generated power.<sup>99,100,103-105,113</sup> In Table 3, significant recent achievements in TE devices are summarized by focusing on conducting polymers, carbon-based materials, and their composites.

As introduced in the previous section, PEDOT is the most popular conducting polymer owing to its high electrical conductivity based on  $\pi$ -conjugated backbone and the delocalized  $\pi$ -electrons.<sup>114</sup> Therefore PEDOT-based conducting polymers have been reported as promising TE materials for application to wearable and flexible TE generators. Especially, PEDOT:PSS have been widely used because of facile processability and stability because the low solubility of PEDOT in aqueous solutions can be improved by emulsification with PSS.<sup>115</sup> As shown in Figure 6(a), Lin *et al.* reported a wearable TE generator with air and moisture permeability.<sup>98</sup> In this report, the  $\sigma$ ,  $\alpha$ , and PF of PEDOT:PSS-coated polyester fabric were  $1.5 \text{ S cm}^{-1}$ ,  $18.5 \mu\text{V K}^{-1}$ , and  $45 \mu\text{W m}^{-1} \text{ K}^{-2}$  at 390 K, respectively. The TE performance could be enhanced by increasing the  $\sigma$  without significant decrease of from 300 to 390 K. The device was based on PEDOT:PSS coated with commercial polyester fabric with silver (Ag) wires as a conductive connection. The TE output voltage and maximum output electrical power were 4.3 mV and 12.29 nW at a  $\Delta T = 75.2 \text{ K}$  using five strips of polyester fabrics as the substrate,

**Table 3.** Summary of TE performances of flexible organic TE devices

Material		PF ( $\mu\text{W m}^{-1} \text{K}^2$ )		$\Delta T^a$	$P_{\max}^b$ ( $\mu\text{W}$ )	$V_{\text{out}}^c$ (mV)	Number of p/n couples	Dimension of a leg (mm <sup>2</sup> or mm <sup>3</sup> )	Fabrication Method	Ref
n-type	p-type	n-type	p-type	(K)						
N/A	Te/PEDOT:PSS	N/A	284	10	0.01059	12.75	16 (legs)	N/A	N/A	9
N/A	PEDOT:PSS	N/A	0.045	75.2	0.01229	4.3	5 (strips)	40×5	Spray doping	98
Cotton thread/Ag paste	Cotton thread/P3HT	N/A	N/A	50	1.15	12	13	4×1×1	Selectable coating	99
CNT/PEI	CNT/FeCl <sub>3</sub>	2456	2387	40	4.2	1.2 (V/g)	60	0.03 (diameter)	Selectable doping	100
CNT/benzylviologen	CNT/FeCl <sub>3</sub>	1.13	1.13	13.9	1.5	5.2	8	4×6×5	Solvent evaporation	101
N/A	CNT/polystyrene	N/A	0.15	70	55 (mW/m <sup>2</sup> )	254 (V/m <sup>2</sup> )	1985 (legs)	1.5×0.8×0.15	Printing	102
SWNT/PEI	SWNT	1500	1840	27.5	2.51	11.3	3	16×10×0.15	Drop-casting, selectable doping	103
PEDOT:PSS/ITO	PEDOT:PSS	N/A	N/A	20	$8.6 \times 10^{-4}$	6.8	8	50×5	Spin coating	104
N/A	PEDOT:PSS	N/A	642	17.5	1	22	24 (strips)	2.75×5	e-Spray method	105
SWNT/DETA/CaH <sub>2</sub>	SWNT	27.7	N/A	55	0.649	62	14	40×10×0.013	Vacuum filtration	106
N/A	PEDOT/H <sub>2</sub> SO <sub>4</sub>	N/A	46.51	51.6	0.1572	7.1	6 (legs)	15×10	Self-assembled Micellar soft-template	107
CNT/DETA/PEBA-Li <sup>+</sup>	CNT/PEBA-Li <sup>+</sup>	543.94	620.22	60	N/A	120	3	30×10	Solution casting	108
SWNT/PEI	urea-SWNTs	50	15	50	0.96	7	4	40×40	Vacuum filtration	109
CNT/PEDOT:PSS/PEI	CNT/PEDOT:PSS	113	83.2	10	0.430	8	12	0.5×15	Wet spinning	110
SWNT/PEI	PEDOT:PSS-coated cotton fabrics	N/A	N/A	60	375	45.2	8	47.5 (mm, length)	Soaking	112
N/A	PEDOT:PSS/NaOH	N/A	N/A	85.5	0.32	52.3	162 (legs)	5×5	Screen printed	113
CNT/benzylviologen	CNT/FeCl <sub>3</sub>	1124	2163	11.7	5.3	40.8	120	5×80	Brush cast doping	118
CNT/PEI	CNT/PVDF	1.47	1.48	28	1.7	N/A	100	31×29×6	Spray doping	119

<sup>a</sup>Temperature difference between hot and cold side. <sup>b</sup>Maximum output power of TE devices. <sup>c</sup>Output voltage of TE devices.

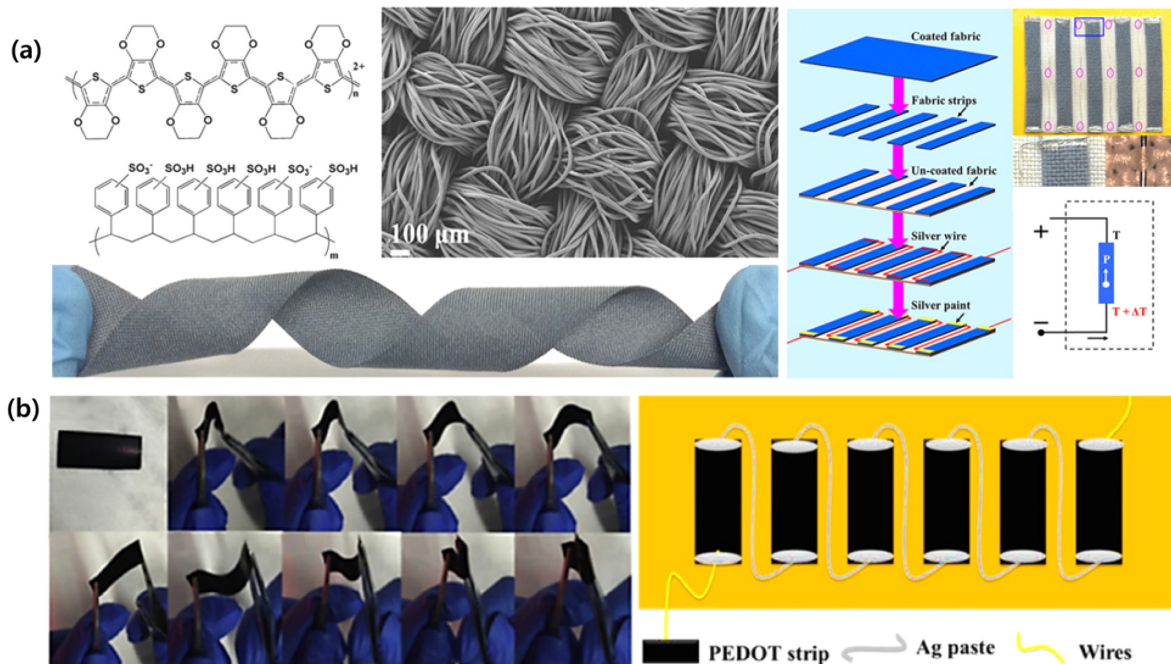


**Figure 6.** Flexible TE modules based on conducting polymers: (a) Polyester fabric coated with PEDOT:PSS and an air-permeable, fabric-based TE generator. Reproduced with permission from Ref. 98, Y. Du *et al.*, *Sci. Rep.*, **5**, 6411 (2015). © 2015, Springer Nature. (b) Free-standing PEDOT nanowire film and the prototype TE module after post-treatment with H<sub>2</sub>SO<sub>4</sub>/NaOH. Reproduced with permission from Ref. 107, D. Ni *et al.*, *Energy*, **170**, 53 (2019). © 2019, Elsevier.

which was coated with PEDOT:PSS. Also, as the strategy to enhance power generation performance of PEDOT-based TE modules, acid (H<sub>2</sub>SO<sub>4</sub>) and base (NaOH) treated-PEDOT nanowire film was used as a p-type TE leg in the report by Cai *et al* (Figure 6(b)).<sup>107</sup>

When processed under optimal post-treatment conditions (6 M H<sub>2</sub>SO<sub>4</sub> followed by 1 M NaOH at room temperature), the  $\alpha$ ,  $\sigma$ , and PF were 25.5  $\mu\text{V K}^{-1}$ , 715.3 S cm<sup>-1</sup>, and 46.51  $\mu\text{W m}^{-1} \text{K}^2$ , respectively. TE performance was improved by 54% compared

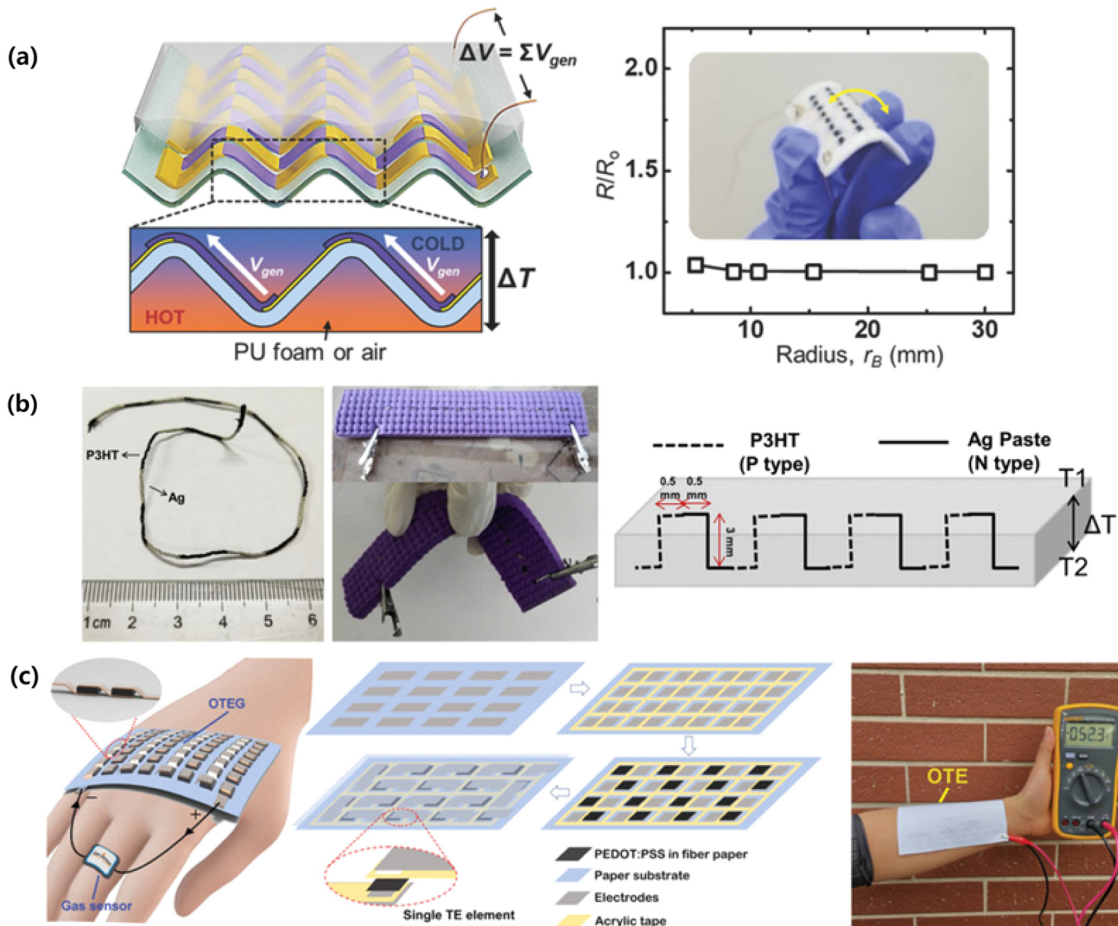


**Figure 7.** TE module designed to operate in response to vertical heat flow: (a) chevron-structured organic TE generator and internal resistance change with respect to the bending radius. Reproduced with permission from Ref. 105, D. Kim *et al.*, *Adv. Mater. Technol.*, **3**, 1700335 (2018). © 2018, John Wiley and Sons. (b) Flexible TE generator structure of fabrics containing cotton thread coated with P3HT and Ag paste. Reproduced with permission from Ref. 99, S. Y. Qu *et al.*, *Thin Solid Films*, **667**, 59 (2018). © 2018, Elsevier. (c) Organic self-powered sensing elements integrating a flexible organic TE generator with a paper substrate and PEDOT:PSS legs. Reproduced with permission from Ref. 113, C. Zheng *et al.*, *Adv. Mater. Technol.*, **4**, 1900247 (2019). © 2019, John Wiley and Sons.

with that of the PEDOT nanowire film before treatment and also had excellent mechanical flexibility, showing that the TE performance of the film was highly stable even after being bent 200 times. The optimal output power was 157.2 nW when six strips of the as-prepared PEDOT nanowire films were connected in series at a temperature difference of 51.6 K.

As a trial to enable flexible TE modules to be practically applied using the normal single heat source such as body heat, the modules were designed to operate in response to vertical heat flow.<sup>99,105,113</sup> Cho *et al.* introduced a PEDOT:PSS-based TE device with a chevron device structure and thermally insulating PU (Figure 7(a)).<sup>105</sup> A PEDOT:PSS/DMSO film was prepared using the electro-spraying process. TE properties were optimized by post-treatment with ethylene glycol to show low sheet resistance ( $< 10 \Omega \text{ sq}^{-1}$ ) and high PF ( $642 \mu\text{W m}^{-1} \text{ K}^2$ ). A chevron-structured TE generator, integrating 24 pairs of PEDOT:PSS films, was mechanically flexible and exhibited TE output power of approximately 1  $\mu\text{W}$  in vertical heat flow with a temperature gradient of 17.5 K. In addition, Yao and Chen *et al.* reported a flexible TE generator by employing P3HT-coated cotton thread as p-type material.<sup>99</sup> The cotton thread coated with P3HT was chemically

doped with Ag paste as the n-type material. The coated TE cotton thread was sewed onto flexible fabrics. The temperature gradient of the device was in the direction of the cross plane of the flexible fabric (Figure 7(b)). As a result, when the temperature gradient was 50 K, the maximum output power was 1.15  $\mu\text{W}$  at the device, which was composed of 13 p- and n-type couples connected in series. Additionally, the TE module, which was designed to be orientated vertically to the heat source, was applied to a flexible self-powered sensor using body heat. Di *et al.* developed a flexible self-powered chemical sensor such as ammonia by integrating a chemical sensing unit based on an organic transistor with a flexible organic TE device (Figure 7(c)).<sup>113</sup> NaOH treated-PEDOT:PSS was used as a single TE element. NaOH doping ratio was optimized to 1 wt%, considering the change of  $\sigma$ ,  $\alpha$  and internal resistance of the TE modules with treatment condition. The TE module was designed to be attached to the human skin with vertical direction from the body heat. Also, the Ag electrode was used as electrode, and Au film was deposited between the Ag electrodes and PEDOT:PSS to reduce the contact resistance between electrodes and legs. The device fabricated with 162 PEDOT:PSS legs indicated the maximum output voltage and

optimized power output at a temperature gradient of 85.5 K were 0.52 V and 0.32  $\mu$ W, corresponding to the internal resistance of 170 k $\Omega$ . Notably, this device could be used to power organic field effect transistor based gas sensors with ultralow operating voltage. This work demonstrated the significant potential for TE devices as flexible power sources for developing self-powered electronics through device integration as a promising candidate for wearable sensing applications.

The hybridization of conducting polymers with inorganic materials has been also investigated to improve the performance of organic flexible TE generators.<sup>9,104</sup> Zhou *et al.* prepared a TE device using PEDOT:PSS as the p-type leg and indium tin oxide (ITO)-PEDOT:PSS as the n-type leg (Figure 8(a)).<sup>104</sup> Deposition of the conducting polymer PEDOT:PSS on top of the ITO served to maintain the mechanical flexibility of ITO. ITO-PEDOT:PSS showed a negative  $\alpha$  value (-14.27  $\mu$ V K<sup>-1</sup>) and slightly lower sheet resistance ( $30.9 \pm 1.8 \Omega \text{ sq}^{-1}$  on PET,  $9.7 \pm 0.2 \Omega \text{ sq}^{-1}$  on glass) than that of ITO film ( $31.4 \pm 1.4 \Omega \text{ sq}^{-1}$  on PET,  $10.6 \pm 0.3 \Omega \text{ sq}^{-1}$  on glass). TE module was fabricated with eight p/n couples of dimensions of 50 mm  $\times$  5 mm. The resistance of the module was  $13.8 \pm 2.1 \text{ k}\Omega$  with eight p/n couples and was linearly dependent on the number of p/n couples with a proportional relationship. The resistance was mainly from low  $\sigma$  (750 S cm<sup>-1</sup>) of PEDOT:PSS as a p-type leg compared with ITO (7280 S cm<sup>-1</sup>). Flexible TE modules could generate a voltage of 6.8 and 11.3 mV and the maximum output power of 0.86 and 1.75 nW at a temperature difference of 20 K and 30K with good mechanical stability and flexibility. Cho *et al.* also reported flexible TE generators by a simple printing process using H<sub>2</sub>SO<sub>4</sub>-treated tellurium-PEDOT:PSS (Te-PEDOT:PSS). TE properties of PEDOT:PSS and Te-PEDOT:PSS hybrid composites were enhanced by H<sub>2</sub>SO<sub>4</sub> post-treatment (Figure 8(b)).<sup>9</sup> The  $\alpha$  of the hybrid composite was enhanced from 10.35 to 250  $\mu$ V K<sup>-1</sup> because of the inherent properties of the Te nanorods. The PF

could be effectively modified, showing the increased value from 68.81 to 284  $\mu$ W m<sup>-1</sup> K<sup>-2</sup> by enhanced  $\sigma$  from 11.01 to 214.86 S cm<sup>-1</sup> with 80 vol% H<sub>2</sub>SO<sub>4</sub> treatment. Besides, Te-PEDOT:PSS solution was printed on a flexible PET substrate to fabricate a flexible TE generator. The TE legs were connected by Ag paste. The maximum power output and the output voltage were 10.59 nW and 12.75 mV, respectively, at 10 K of temperature difference. The TE generators also exhibited a stable TE voltage of over 2 mV in response to human body heat.

The hybridization of a conducting polymer with carbon nanotubes (CNTs) has been also considered as a promising method for enhancing the TE performance.<sup>100,110,116</sup> The reason is because the contribution of the CNTs to the  $\sigma$  could be increased in these composite films, thereby improving the PF while maintaining the low thermal conductivity.<sup>102,117,118</sup> Cho and Jiang *et al.* reported an organic fiber TE generator using CNT/PEDOT:PSS composite fibers (Figure 9(a)), which were prepared by a wet-spinning process.<sup>110</sup> The TE performance of p- and n-type composites was improved by using post-processing with hydrazine and polyethyleneimine (PEI). The optimized p- and n-type PFs were  $83.2 \pm 6.4$  and  $113 \pm 25 \mu$ W m<sup>-1</sup> K<sup>-2</sup> with enhanced  $\sigma$ . The maximum output power was 0.430  $\mu$ W at a temperature difference of 10 K when the organic fiber TE generator was assembled with 12 couples of p- and n-type TE fibers. Liu, Xu, and Jiang *et al.* assembled a flexible fiber-based TE generator by connecting p-type PEDOT:PSS-coated common cotton fabric (CNF) (CNF@PP) and n-type CNT (n-CNT) fibers in series (Figure 9(b)).<sup>112</sup> PDMS was used as a protective layer to provide isolation from air to avoid oxidation of the n-CNTs. The CNF@PP was prepared by using a simple soaking method with DMSO. A high  $\sigma$  of 18.8 and 871 S cm<sup>-1</sup> was achieved in CNF@PP and n-CNTs, respectively. At a temperature gradient of 60 K, the output voltage and output power of the TE device with eight p/n couples in the non-stretched

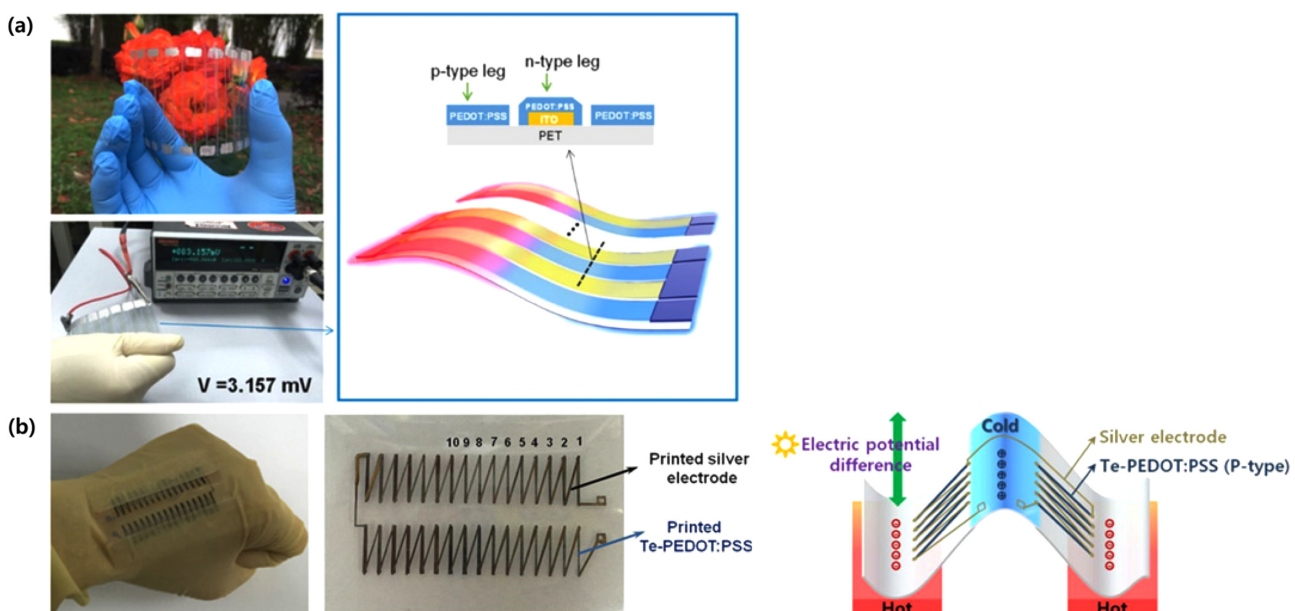


**Figure 8.** Hybridization of conducting polymer with inorganic materials. (a) Flexible and transparent PEDOT:PSS-based organic-inorganic hybrid TE module on PET. Reproduced with permission from Ref. 104, X. Dong *et al.*, *ACS Appl. Mater. Interfaces*, **10**, 26687 (2018). © 2018, American Chemical Society. (b) Flexible TE generator using Te-PEDOT:PSS hybrid composite. Reproduced with permission from Ref. 9, E. Bae *et al.*, *Sci. Rep.*, **6**, 18805 (2016). © 2016, Springer Nature.

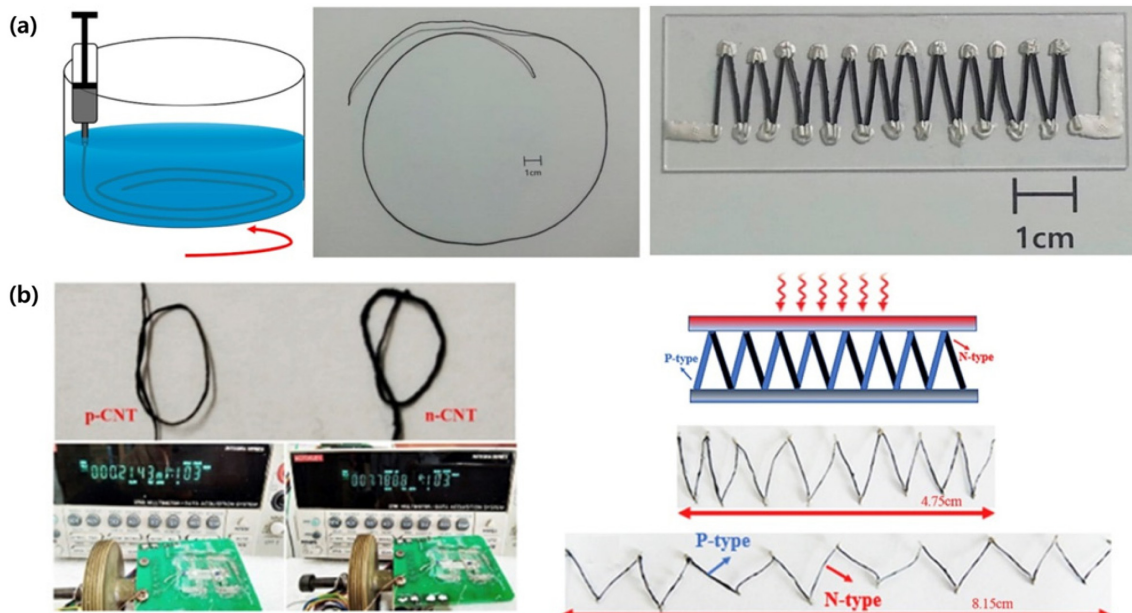


**Figure 9.** Hybridization of a conducting polymer with CNT: (a) CNT/PEDOT:PSS composite fiber and the organic fiber TE generator. Reproduced with permission from Ref. 110, J. Y. Kim *et al.*, *Carbon*, **133**, 293 (2018). © 2018, Elsevier. (b) Fiber-based TE generator with eight p/n couples of CNF@PP and n-type CNT. Reproduced with permission from Ref. 112, X. Q. Lan *et al.*, *Compos. Sci. Technol.*, **182**, 107767 (2019). © 2019, Elsevier.

state were 39 mV and 290  $\mu$ W with 935  $\Omega$  of internal resistance, respectively. Interestingly, when it was stretched out, the output voltage and output power were increased to 45.2 mV and 375  $\mu$ W, providing insight into the assembly of wearable all organic TE generators.

Additionally, owing to their high  $\sigma$  and mechanical flexibility, CNTs can be potentially used in flexible organic TE devices.<sup>101,102,109</sup> CNTs and their composites with polymer represent a large por-

tion of organic TE researches, because of the remarkable increase in the value of ZT.<sup>119</sup> Pristine semiconducting CNTs show a p-type behavior because of oxygen doping during their synthesis in air atmosphere.<sup>120</sup> Many developments involving the application of p-type CNT semiconductors in flexible TE generators have been reported.<sup>117,121</sup> However, n-type CNT materials have been investigated to a limited extent. Lee *et al.* reported a CNT-based organic TE device to overcome the drawback of the low

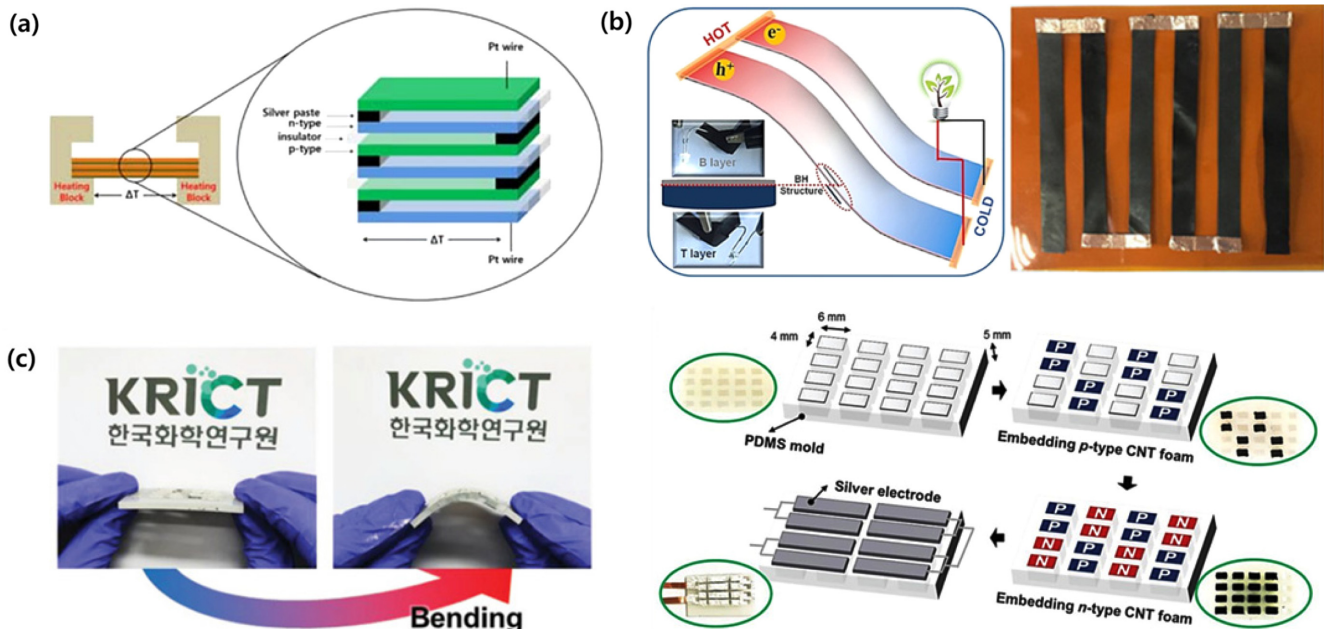


**Figure 10.** Flexible TE modules based on doped CNTs: (a) Flexible TE module fabricated by stacking p- and n-type SWCNTs alternately with insulating layers. Reproduced with permission from Ref. 109, H. Bark *et al.*, *Macromol. Res.*, **23**, 795 (2015). © 2015, Springer Nature. (b) Bilayer heterogeneous structured flexible module with CNT/PEBA-Li<sup>+</sup> based films. Reproduced with permission from Ref. 108, T. Luo *et al.*, *ACS Appl. Energy Mater.*, **1**, 1904 (2018). © 2018, American Chemical Society. (c) TE device fabricated with optimized p-/n-doped CNT foams. Reproduced with permission from Ref. 101, M. Lee *et al.*, *Adv. Energy Mater.*, **9**, 1900914 (2019). © 2019, John Wiley and Sons.

$\sigma$  of organic TE devices.<sup>109</sup> In this work, as p-typed TE materials, the urea-treated SWCNTs yielded a maximum PF of  $15 \mu\text{W m}^{-1}\text{K}^2$  at 380 K. The n-type material prepared from PEI-SWCNTs generated a PF of  $50 \mu\text{W m}^{-1}\text{K}^2$  at 380 K. As shown in Figure 10(a), the flexible TE modules were fabricated by stacking the prepared p- and n-type films alternately between insulating layers. In terms of the TE performance, the TE voltage with four p/n couples reached 7 mV at a temperature gradient of 50 K. Because of their low electrical resistance formed by well-percolated networks of SWCNTs, the maximum power of 960 nW was generated. Pan *et al.* used the block copolymer poly(ether-b-amide12) (PEBA) with excellent flexibility and mechanical properties to fabricate TE materials by blending with CNTs (Figure 10(b)).<sup>108</sup> After doping the PEBA with lithium chloride (PEBA-Li<sup>+</sup>), two types (p- and n-type) of CNT-filled PEBA-Li<sup>+</sup> (CNT-PEBA-Li<sup>+</sup>) TE composites were obtained *via* a simple one-step casting method. The n-type CNT was obtained by using diethylenetriamine (DETA) as a dopant. The TE module was fabricated by stacking bilayer heterogeneous structures of thermally nonconductive and conductive layers. The results showed that the TE voltage of the module consisting of three p/n couples was able to reach 120 mV at a temperature gradient of 60 K. In addition, Cho *et al.* reported that a TE generator was fabricated from CNT foam with a porous structure.<sup>101</sup> The ultralow

thermal conductivity of  $0.17 \text{ W m}^{-1}\text{K}^{-1}$  together with the extremely high porosity (above 90%) was considered to be the main reason for the enhanced TE performance. The highly porous structure of CNT foam contributed to the enhancement of phonon scattering which yielded thermal conductivity 100 times lower than that of a CNT film with a densely packed network. As shown in Figure 10(c), a TE device fabricated with optimized p- and n-doped CNT foams exhibited optimal output power ( $1.5 \mu\text{W}$ ) and output power per weight ( $82 \mu\text{W g}^{-1}$ ), respectively, at a temperature gradient of 13.9 K.

Another important parameter to increase the TE performance is to optimize the electrical connection between TE materials, because contact resistance between the TE materials and the electrode can impede the performance. Therefore, electrode-free TE devices have drawn much attention. Kim and Park *et al.* reported an ultralight flexible device based on carbon nanotube yarn (CNTY), as shown in Figure 11(a), which solved the problem of high contact resistance.<sup>100</sup> The prepared CNTY was divided into three parts, the n-type part doped with PEI, p-type part doped with FeCl<sub>3</sub>, and the undoped CNTY was used as the electrode instead of the traditional metal electrode to minimize the circuit resistance. This structure exhibited superior  $\sigma$  of  $3147 \text{ S cm}^{-1}$  owing to increased longitudinal carrier mobility derived from the highly aligned structure. The circuit resistance of

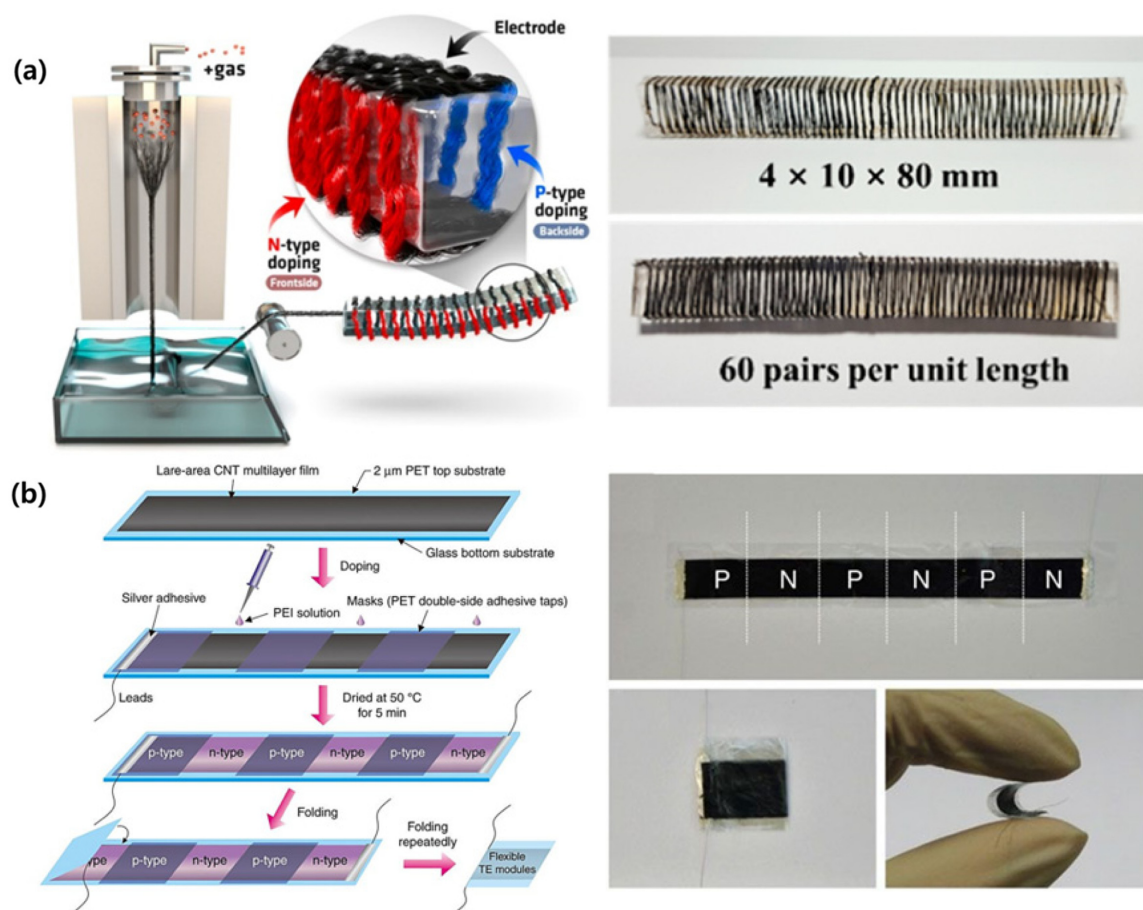


**Figure 11.** Metal electrode-free TE modules between n- and p-type legs with selective doping process. (a) Fabrication of the CNTY and flexible TE generator based on CNTY. Reproduced with permission from Ref. 100, J. Choi *et al.*, *ACS Nano*, **11**, 7608 (2017). © 2017, American Chemical Society. (b) Compact flexible TE modules with novel configuration with CNT-based TE materials with a selectable doping process. Reproduced with permission from Ref. 103, W. Zhou *et al.*, *Nat. Commun.*, **8**, 14886 (2017). © 2017, Springer Nature.

flexible TE generators with and without Ag paste as the electrode was 27 and  $21\ \Omega$ .<sup>100</sup> The corresponding TE device based on 60 couples of p-/n-doped CNTY had a maximum power density of 1.3 and  $4.2\ \mu\text{W}$  at temperature differences of 5 and 40 K, respectively. Zhou and Xie *et al.* also reported a technique to fabricate compact flexible TE modules with a novel configuration (Figure 11(b)).<sup>103</sup> The large-area continuous CNT film was synthesized via the floating catalyst chemical vapor deposition method. A CNT strip ( $96 \times 10\ \text{mm}^2$ ) from the synthesized film was placed on PET substrate. PEI solution was dropped onto the prepared CNT strip for localized n-type doping in the unshaded area of the strip with an alternately designed mask. The optimized n-type film exhibited an ultrahigh PF of  $\sim 1,500\ \mu\text{W m}^{-1}\ \text{K}^{-2}$  and outstanding stability in air without additional encapsulation. The open-circuit voltage, maximum output power, and power density of this CNT module with three couples were 11.3 mV,  $2.51\ \mu\text{W}$ , and  $167\ \text{mW cm}^{-2}$  with small internal resistance of  $12.5\ \Omega$ , respectively. It is worth mentioning that this technique could possibly be used in large-scale synthesis and mass production in combination with a technique capable of direct and high-yield synthesis of continuous CNT films.

## 6. Conclusions

Recently, organic TE generators have achieved remarkable advancements by extensive studies on p- and n-type materials design, new dopants and doping methods, morphology control in doped films and optimization of device architectures. By tailoring post-treatments, PEDOT:PSS showed the highest ZT value of 0.75, demonstrating a similar TE performance to inorganic counterparts at room temperature. n-Type organic TE materials have also achieved the highest ZT up to  $\sim 0.2$ , which is still poorer compared to p-type ones due to their poor air stability and  $\sigma$ . It is important to explore further the new candidates of p- and n-type TE materials for improving TE performances. Systematic approaches are continuously required including structural engineering of conjugated backbones and substituted side-chains, and tailoring doping methodology. Developing new dopants are also necessary which can fine-modulate the carrier concentration in the doped organic materials without disturbing original crystalline film morphology. The  $\sigma$  and  $\alpha$  have a trade-off relationship depending on the carrier concentration: as the carrier density increases,  $\sigma$  increases, but  $\alpha$  decreases. Thus, it is important to precisely control the amount of doping concentration to achieve the maximum PF. Decoupling the trade-off relationship of  $\sigma$  and  $\alpha$  needs to be also investigated for further improving the PF. In addition, the charge transport properties in the doped TE polymers (and small molecules) are not well understood at a present stage. It is challenging to precisely measure the carriers concentration and their mobility in doped materials, which makes it difficult to optimize the TE performance. Currently, the several charge transport models which were originally developed for inorganic systems, are applied to organic TE systems with some modifications, showing a limited interpretation for the charge transport behaviors in organic materials. A new theoretical model specialized for organic TE systems are necessary to be developed.

Flexible organic TE devices, which have been gaining the growing scientific interests, are a promising candidate as renewable energy sources, especially in the application of energy harvesting for flexible and wearable devices based on human body temperature. The combination of organic TE materials with textile-based clothing as well as a flexible heat sink for smart fashion becomes a new tendency of the wearable device. However, the TE power generation performances of organic TE generators are much lower compared to conventional inorganic devices based on  $\text{Bi}_2\text{Te}_3$ , PbTe, SbTe, and so on, which is attributed to the smaller ZT values of organic TE materials and the high contact resistance between the organic semiconductor layer and metal electrodes, as well as limited device configurations for the high-temperature gradient TE energy conversion. To further enhance the TE performances of organic TE generators, a careful attention should be also directed to the device integration which decreases the contact resistance by interface engineering between TE layers and electrodes as well as developments of new novel flexible electrode materials. A new architecture design for conformal thermal contact on the hot surface of heat source is also required for efficient thermal transport and large temperature gradient generation in organic TE devices. By considering the potentials and advantages of organic TE generators compared to inorganic counterparts, intensive studies should be directed toward opening plausible real applications of organic TE devices.

## References

- (1) C. X. Wei, L. H. Wang, C. J. Pan, Z. M. Chen, H. B. Zhao, and L. Wang, *React. Funct. Polym.*, **142**, 1 (2019).
- (2) P. Ren, Y. M. Liu, J. He, T. Lv, J. L. Gao, and G. Y. Xu, *Inorg. Chem. Front.*, **5**, 2380 (2018).
- (3) T. J. Seebeck, *Ueber den Magnetismus der Galvanischen Kette*, 1822.
- (4) J. C. Peltier, *Ann. Chim. Phys.*, **56**, 371 (1834).
- (5) J. P. Heremans, V. Jovovic, E. S. Toberer, A. Saramat, K. Kurosaki, A. Charoenphakdee, S. Yamanaka, and G. J. Snyder, *Science*, **321**, 554 (2008).
- (6) H. Ohta, S. Kim, Y. Mune, T. Mizoguchi, K. Nomura, S. Ohta, T. Nomura, Y. Nakanishi, Y. Ikuhara, and M. Hirano, *Nat. Mater.*, **6**, 129 (2007).
- (7) G. J. Snyder and A. H. Snyder, *Energy Environ. Sci.*, **10**, 2280 (2017).
- (8) H. J. Goldsmid, *Proc. Phys. Soc. Lond.*, **71**, 633 (1958).
- (9) E. J. Bae, Y. H. Kang, K. S. Jang, and S. Y. Cho, *Sci. Rep.*, **6**, 18805 (2016).
- (10) A. I. Boukai, Y. Bunimovich, J. Tahir-Kheli, J. K. Yu, W. A. Goddard, 3rd, and J. R. Heath, *Nature*, **451**, 168 (2008).
- (11) Z. H. Dugaish, *Physica B*, **322**, 205 (2002).
- (12) L. D. Zhao, S. H. Lo, Y. Zhang, H. Sun, G. Tan, C. Uher, C. Wolverton, V. P. Dravid, and M. G. Kanatzidis, *Nature*, **508**, 373 (2014).
- (13) B. Russ, A. Glaudell, J. J. Urban, M. L. Chabiny, and R. A. Segalman, *Nat. Rev. Mater.*, **1**, 16050 (2016).
- (14) B. T. McGrail, A. Sehirlioglu, and E. Pentzer, *Angew. Chem. Int. Ed. Engl.*, **54**, 1710 (2015).
- (15) D. Huang, H. Yao, Y. Cui, Y. Zou, F. Zhang, C. Wang, H. Shen, W. Jin, J. Zhu, Y. Diao, W. Xu, C. A. Di, and D. Zhu, *J. Am. Chem. Soc.*, **139**, 13013 (2017).
- (16) Z. Fan, D. H. Du, X. Guan, and J. Y. Ouyang, *Nano Energy*, **51**, 481 (2018).
- (17) T. Park, C. Park, B. Kim, H. Shin, and E. Kim, *Energy Environ. Sci.*, **6**, 788 (2013).
- (18) K. Chang, M. Jeng, C. Yang, Y. Chou, S. Wu, M. A. Thomas, and Y. Peng, *J. Electron. Mater.*, **38**, 1182 (2009).

- (19) O. Bubnova, M. Berggren, and X. Crispin, *J. Am. Chem. Soc.*, **134**, 16456 (2012).
- (20) J. J. Luo, D. Billep, T. Waechtler, T. Otto, M. Toader, O. Gordan, E. Sheremet, J. Martin, M. Hietschold, D. R. T. Zahnd, and T. Gessner, *J. Mater. Chem. A*, **1**, 7576 (2013).
- (21) G. H. Kim, L. Shao, K. Zhang, and K. P. Pipe, *Nat. Mater.*, **12**, 719 (2013).
- (22) H. Park, S. H. Lee, F. S. Kim, H. H. Choi, I. W. Cheong, and J. H. Kim, *J. Mater. Chem. A*, **2**, 6532 (2014).
- (23) C. Yi, A. Wilhite, L. Zhang, R. Hu, S. S. Chuang, J. Zheng, and X. Gong, *ACS Appl. Mater. Interfaces*, **7**, 8984 (2015).
- (24) Z. Fan, P. C. Li, D. H. Du, and J. Y. Ouyang, *Adv. Energy Mater.*, **7**, 1602116 (2017).
- (25) M. Culebras, C. M. Gomez, and A. Cantarero, *J. Mater. Chem. A*, **2**, 10109 (2014).
- (26) O. Bubnova, Z. U. Khan, A. Malti, S. Braun, M. Fahlman, M. Berggren, and X. Crispin, *Nat. Mater.*, **10**, 429 (2011).
- (27) O. Bubnova, Z. U. Khan, H. Wang, S. Braun, D. R. Evans, M. Fabretto, P. Hojati-Talemi, D. Dagnelund, J. B. Arlin, Y. H. Geerts, S. Desbief, D. W. Breiby, J. W. Andreasen, R. Lazzaroni, W. M. Chen, I. Zozoulenko, M. Fahlman, P. J. Murphy, M. Berggren, and X. Crispin, *Nat. Mater.*, **13**, 190 (2014).
- (28) M. L. Chabinyc, M. F. Toney, R. J. Kline, I. McCulloch, and M. Heeney, *J. Am. Chem. Soc.*, **129**, 3226 (2007).
- (29) Q. Zhang, Y. M. Sun, W. Xu, and D. B. Zhu, *Macromolecules*, **47**, 609 (2014).
- (30) S. N. Patel, A. M. Glaudell, D. Kiefer, and M. L. Chabinyc, *ACS Macro Lett.*, **5**, 268 (2016).
- (31) S. N. Patel, A. M. Glaudell, K. A. Peterson, E. M. Thomas, K. A. O'Hara, E. Lim, and M. L. Chabinyc, *Sci. Adv.*, **3**, e1700434 (2017).
- (32) Q. Zhang, Y. M. Sun, W. Xu, and D. B. Zhu, *Energy. Environ. Sci.*, **5**, 9639 (2012).
- (33) C. T. Hong, Y. Yoo, Y. H. Kang, J. Ryu, S. Y. Cho, and K. S. Jang, *RSC Adv.*, **5**, 11385 (2015).
- (34) I. H. Jung, C. T. Hong, U. H. Lee, Y. H. Kang, K. S. Jang, and S. Y. Cho, *Sci. Rep.*, **7**, 44704 (2017).
- (35) R. B. Aich, N. Blouin, A. Bouchard, and M. Leclerc, *Chem. Mater.*, **21**, 751 (2009).
- (36) S. A. Gregory, A. K. Menon, S. Ye, D. S. Seferos, J. R. Reynolds, and S. K. Yee, *Adv. Energy Mater.*, **8**, 1802419 (2018).
- (37) J. Ding, Z. Liu, W. Zhao, W. Jin, L. Xiang, Z. Wang, Y. Zeng, Y. Zou, F. Zhang, Y. Yi, Y. Diao, C. R. McNeill, C. A. Di, D. Zhang, and D. Zhu, *Angew. Chem. Int. Ed. Engl.*, **58**, 18994 (2019).
- (38) Y. Joo, L. F. Huang, N. Eedugurala, A. E. London, A. Kumar, B. M. Wong, B. W. Boudouris, and J. D. Azoulay, *Macromolecules*, **51**, 3886 (2018).
- (39) T. L. D. Tam, C. K. Ng, S. L. Lim, E. Yildirim, J. Ko, W. L. Leong, S. W. Yang, and J. W. Xu, *Chem. Mater.*, **31**, 8543 (2019).
- (40) J. Park, Y. Lee, M. Kim, Y. Kim, A. Tripathi, Y. W. Kwon, J. Kwak, and H. Y. Woo, *ACS Appl. Mater. Interfaces*, **12**, 1110 (2020).
- (41) T. L. D. Tam, G. Wu, S. W. Chien, S. F. V. Lim, S.-W. Yang, and J. Xu, *ACS Mater. Lett.*, **2**, 147 (2020).
- (42) E. H. Suh, Y. J. Jeong, J. G. Oh, K. Lee, J. Jung, Y. S. Kang, and J. Jang, *Nano Energy*, **58**, 585 (2019).
- (43) Y. Karpov, T. Erdmann, I. Raguzin, M. Al-Hussein, M. Binner, U. Lappan, M. Stamm, K. L. Gerasimov, T. Beryozkina, V. Bakulev, D. V. Anokhin, D. A. Ivanov, F. Gunther, S. Gemming, G. Seifert, B. Voit, R. Di Pietro, and A. Kiriy, *Adv. Mater.*, **28**, 6003 (2016).
- (44) R. Kroon, D. Kiefer, D. Stegerer, L. Yu, M. Sommer, and C. Muller, *Adv. Mater.*, **29**, 1700930 (2017).
- (45) J. Lee, J. Kim, T. L. Nguyen, M. Kim, J. Park, Y. Lee, S. Hwang, Y. W. Kwon, J. Kwak, and H. Y. Woo, *Macromolecules*, **51**, 3360 (2018).
- (46) R. Kroon, D. A. Mengistie, D. Kiefer, J. Hyynnen, J. D. Ryan, L. Yu, and C. Muller, *Chem. Soc. Rev.*, **45**, 6147 (2016).
- (47) P. Wei, T. Menke, B. D. Naab, K. Leo, M. Riede, and Z. Bao, *J. Am. Chem. Soc.*, **134**, 3999 (2012).
- (48) H. E. Katz, J. Johnson, A. J. Lovinger, and W. J. Li, *J. Am. Chem. Soc.*, **122**, 7787 (2000).
- (49) H. Yan, Z. Chen, Y. Zheng, C. Newman, J. R. Quinn, F. Dotz, M. Kastler, and A. Facchetti, *Nature*, **457**, 679 (2009).
- (50) R. A. Schlitz, F. G. Brunetti, A. M. Glaudell, P. L. Miller, M. A. Brady, C. J. Takacs, C. J. Hawker, and M. L. Chabinyc, *Adv. Mater.*, **26**, 2825 (2014).
- (51) J. Liu, L. Qiu, R. Alessandri, X. Qiu, G. Portale, J. Dong, W. Talsma, G. Ye, A. A. Sengrian, P. C. T. Souza, M. A. Loi, R. C. Chiechi, S. J. Marrink, J. C. Hummelen, and L. J. A. Koster, *Adv. Mater.*, **30**, 1704630 (2018).
- (52) A. Giovannitti, C. B. Nielsen, D. T. Sbircea, S. Inal, M. Donahue, M. R. Niazi, D. A. Hanifi, A. Amassian, G. G. Malliaras, J. Rivnay, and I. McCulloch, *Nat. Commun.*, **7**, 13066 (2016).
- (53) D. Kiefer, A. Giovannitti, H. Sun, T. Biskup, A. Hofmann, M. Koopmans, C. Cendra, S. Weber, L. J. Anton Koster, E. Olsson, J. Rivnay, S. Fabiano, I. McCulloch, and C. Muller, *ACS Energy Lett.*, **3**, 278 (2018).
- (54) J. Liu, G. Ye, B. V. Zee, J. Dong, X. Qiu, Y. Liu, G. Portale, R. C. Chiechi, and L. J. A. Koster, *Adv. Mater.*, **30**, 1804290 (2018).
- (55) S. Wang, H. Sun, U. Ail, M. Vagin, P. O. Persson, J. W. Andreasen, W. Thiel, M. Berggren, X. Crispin, D. Fazzi, and S. Fabiano, *Adv. Mater.*, **28**, 10764 (2016).
- (56) Y. Wang, M. Nakano, T. Michinobu, Y. Kiyota, T. Mori, and K. Takimiyama, *Macromolecules*, **50**, 857 (2017).
- (57) T. Lei, J. H. Dou, X. Y. Cao, J. Y. Wang, and J. Pei, *J. Am. Chem. Soc.*, **135**, 12168 (2013).
- (58) T. Lei, J. H. Dou, X. Y. Cao, J. Y. Wang, and J. Pei, *Adv. Mater.*, **25**, 6589 (2013).
- (59) K. Shi, F. Zhang, C. A. Di, T. W. Yan, Y. Zou, X. Zhou, D. Zhu, J. Y. Wang, and J. Pei, *J. Am. Chem. Soc.*, **137**, 6979 (2015).
- (60) X. Zhao, D. Madan, Y. Cheng, J. Zhou, H. Li, S. M. Thon, A. E. Bragg, M. E. DeCoster, P. E. Hopkins, and H. E. Katz, *Adv. Mater.*, **29**, 1606928 (2017).
- (61) C. Y. Yang, W. L. Jin, J. Wang, Y. F. Ding, S. Nong, K. Shi, Y. Lu, Y. Z. Dai, F. D. Zhuang, T. Lei, C. A. Di, D. Zhu, J. Y. Wang, and J. Pei, *Adv. Mater.*, **30**, 1802850 (2018).
- (62) H. I. Un, S. A. Gregory, S. K. Mohapatra, M. Xiong, E. Longhi, Y. Lu, S. Rigin, S. Jhulkki, C. Y. Yang, T. V. Timofeeva, J. Y. Wang, S. K. Yee, S. Barlow, S. R. Marder, and J. Pei, *Adv. Energy. Mater.*, **9**, 1900817 (2019).
- (63) Y. Lu, Z. D. Yu, R. Z. Zhang, Z. F. Yao, H. Y. You, L. Jiang, H. I. Un, B. W. Dong, M. Xiong, J. Y. Wang, and J. Pei, *Angew. Chem. Int. Ed. Engl.*, **58**, 11390 (2019).
- (64) A. Hamidi-Sakr, L. Biniek, J. L. Bantignies, D. Maurin, L. Herrmann, N. Leclerc, P. Leveque, V. Vijayakumar, N. Zimmermann, and M. Brinkmann, *Adv. Funct. Mater.*, **27**, 1700173 (2017).
- (65) S. Hwang, W. J. Potscavage, R. Nakamichi, and C. Adachi, *Org. Electron.*, **31**, 31 (2016).
- (66) T. P. Kaloni, P. K. Giesbrecht, G. Schreckenbach, and M. S. Freund, *Chem. Mater.*, **29**, 10248 (2017).
- (67) P. Wei, J. H. Oh, G. Dong, and Z. Bao, *J. Am. Chem. Soc.*, **132**, 8852 (2010).
- (68) A. Jha, H. G. Duan, V. Tiwari, M. Thorwart, and R. J. D. Miller, *Chem. Sci.*, **9**, 4468 (2018).
- (69) D. Kiefer, L. Yu, E. Fransson, A. Gomez, D. Primetzhofer, A. Amassian, M. Campoy-Quiles, and C. Muller, *Adv. Sci. (Weinh.)*, **4**, 1600203 (2017).
- (70) D. T. Scholes, S. A. Hawks, P. Y. Yee, H. Wu, J. R. Lindemuth, S. H. Tolbert, and B. J. Schwartz, *J. Phys. Chem. Lett.*, **6**, 4786 (2015).
- (71) L. Muller, D. Nanova, T. Glaser, S. Beck, A. Pucci, A. K. Kast, R. R. Schroder, E. Mankel, P. Pingel, D. Neher, W. Kowalsky, and R. Lovrincic, *Chem. Mater.*, **28**, 4432 (2016).
- (72) S. E. Yoon, Y. Kang, S. Y. Noh, J. Park, S. Y. Lee, J. Park, D. W. Lee, D. R. Whang, T. Kim, G. H. Kim, H. Seo, B. G. Kim, and J. H. Kim, *ACS Appl. Mater. Interfaces*, **12**, 1151 (2020).
- (73) A. Mazaheripour, E. M. Thomas, R. A. Segalman, and M. L. Chabinyc, *Macromolecules*, **52**, 2203 (2019).
- (74) M. T. Fontana, D. A. Stanfield, D. T. Scholes, K. J. Winchell, S. H. Tol-

- bert, and B. J. Schwartz, *J. Phys. Chem. C*, **123**, 22711 (2019).
- (75) E. E. Perry, C. Y. Chiu, K. Moudgil, R. A. Schlitz, C. J. Takacs, K. A. O'Hara, J. G. Labram, A. M. Glaudell, J. B. Sherman, S. Barlow, C. J. Hawker, S. R. Marder, and M. L. Chabinyc, *Chem. Mater.*, **29**, 9742 (2017).
- (76) I. E. Jacobs, E. W. Aasen, J. L. Oliveira, T. N. Fonseca, J. D. Roehling, J. Li, G. W. Zhang, M. P. Augustine, M. Mascal, and A. J. Moule, *J. Mater. Chem. C*, **4**, 3454 (2016).
- (77) A. R. Chew, R. Ghosh, Z. Shang, F. C. Spano, and A. Salleo, *J. Phys. Chem. Lett.*, **8**, 4974 (2017).
- (78) E. Lim, K. A. Peterson, G. M. Su, and M. L. Chabinyc, *Chem. Mater.*, **30**, 998 (2018).
- (79) Y. Lu, J. Y. Wang, and J. Pei, *Chem. Mater.*, **31**, 6412 (2019).
- (80) S. D. Kang and G. J. Snyder, *Nat. Mater.*, **16**, 252 (2017).
- (81) N. Mott, *J. Phys. C Solid State*, **20**, 3075 (1987).
- (82) A. M. Glaudell, J. E. Cochran, S. N. Patel, and M. L. Chabinyc, *Adv. Energy Mater.*, **5**, 1401072 (2015).
- (83) H. Fritzsche, *Solid State Commun.*, **9**, 1813 (1971).
- (84) E. A. Davis and N. Mott, *Electronic Processes in Non-Crystalline Materials*, Oxford University Press, 1971.
- (85) V. Ambegaokar, B. I. Halperin, and J. S. Langer, *Phys. Rev. B Condens. Matter*, **4**, 2612 (1971).
- (86) M. Z. Ansari and N. Khare, *J. Appl. Phys.*, **117**, 025706 (2015).
- (87) A. Miller and E. Abrahams, *Phys. Rev.*, **120**, 745 (1960).
- (88) M. J. Panzer and C. D. Frisbie, *Adv. Funct. Mater.*, **16**, 1051 (2006).
- (89) R. Noriega, J. Rivnay, K. Vandewal, F. P. Koch, N. Stingelin, P. Smith, M. F. Toney, and A. Salleo, *Nat. Mater.*, **12**, 1038 (2013).
- (90) M. He, J. Li, M. L. Sorensen, F. Zhang, R. R. Hancock, H. H. Fong, V. A. Pozdin, D. M. Smilgies, and G. G. Malliaras, *J. Am. Chem. Soc.*, **131**, 11930 (2009).
- (91) I. McCulloch, M. Heeney, C. Bailey, K. Genevicius, I. Macdonald, M. Shkunov, D. Sparrowe, S. Tierney, R. Wagner, W. Zhang, M. L. Chabinyc, R. J. Kline, M. D. McGehee, and M. F. Toney, *Nat. Mater.*, **5**, 328 (2006).
- (92) H. Li, M. E. DeCoster, R. M. Ireland, J. Song, P. E. Hopkins, and H. E. Katz, *J. Am. Chem. Soc.*, **139**, 11149 (2017).
- (93) H. Li, E. Plunkett, Z. X. Cai, B. T. Qiu, T. R. Wei, H. Y. Chen, S. M. Thon, D. H. Reich, L. D. Chen, and H. E. Katz, *Adv. Electron. Mater.*, **5**, 1800618 (2019).
- (94) G. Z. Zuo, Z. J. Li, E. G. Wang, and M. Kemerink, *Adv. Electron. Mater.*, **4**, 1700501 (2018).
- (95) B. Kim, H. Shin, T. Park, H. Lim, and E. Kim, *Adv. Mater.*, **25**, 5483 (2013).
- (96) X. Wang, X. Zhang, L. Sun, D. Lee, S. Lee, M. Wang, J. Zhao, Y. Shao-Horn, M. Dinca, T. Palacios, and K. K. Gleason, *Sci. Adv.*, **4**, eaat5780 (2018).
- (97) C. J. Boyle, M. Upadhyaya, P. Wang, L. A. Renna, M. Lu-Diaz, S. Pyo Jeong, N. Hight-Huf, L. Korugic-Karasz, M. D. Barnes, Z. Aksamija, and D. Venkataraman, *Nat. Commun.*, **10**, 2827 (2019).
- (98) Y. Du, K. Cai, S. Chen, H. Wang, S. Z. Shen, R. Donelson, and T. Lin, *Sci. Rep.*, **5**, 6411 (2015).
- (99) S. Y. Qu, Y. L. Chen, W. Shi, M. D. Wang, Q. Yao, and L. D. Chen, *Thin Solid Films*, **667**, 59 (2018).
- (100) J. Choi, Y. Jung, S. J. Yang, J. Y. Oh, J. Oh, K. Jo, J. G. Son, S. E. Moon, C. R. Park, and H. Kim, *ACS Nano*, **11**, 7608 (2017).
- (101) M. H. Lee, Y. H. Kong, J. Kim, Y. K. Lee, and S. Y. Cho, *Adv. Energy Mater.*, **9**, 1900914 (2019).
- (102) K. Suemori, S. Hoshino, and T. Kamata, *Appl. Phys. Lett.*, **103**, 153902 (2013).
- (103) W. Zhou, Q. Fan, Q. Zhang, L. Cai, K. Li, X. Gu, F. Yang, N. Zhang, Y. Wang, H. Liu, W. Zhou, and S. Xie, *Nat. Commun.*, **8**, 14886 (2017).
- (104) X. Dong, S. Xiong, B. Luo, R. Ge, Z. Li, J. Li, and Y. Zhou, *ACS Appl. Mater. Interfaces*, **10**, 26687 (2018).
- (105) D. Kim, D. Ju, and K. Cho, *Adv. Mater. Technol.*, **3**, 1700335 (2018).
- (106) G. B. Wu, C. Y. Gao, G. M. Chen, X. Wang, and H. F. Wang, *J. Mater. Chem. A*, **4**, 14187 (2016).
- (107) D. Ni, H. J. Song, Y. X. Chen, and K. F. Cai, *Energy*, **170**, 53 (2019).
- (108) T. Luo and K. Pan, *ACS Appl. Energy Mater.*, **1**, 1904 (2018).
- (109) H. Bark, W. Lee, and H. Lee, *Macromol. Res.*, **23**, 795 (2015).
- (110) J. Y. Kim, W. Lee, Y. H. Kang, S. Y. Cho, and K. S. Jang, *Carbon*, **133**, 293 (2018).
- (111) O. Bubnova and X. Crispin, *Energ. Environ. Sci.*, **5**, 9345 (2012).
- (112) X. Q. Lan, T. Z. Wang, C. C. Liu, P. P. Liu, J. K. Xu, X. F. Liu, Y. K. Du, and F. X. Jiang, *Compos. Sci. Technol.*, **182**, 107767 (2019).
- (113) C. Zheng, L. Xiang, W. Jin, H. Shen, W. Zhao, F. Zhang, C. A. Di, and D. Zhu, *Adv. Mater. Technol.*, **4**, 1900247 (2019).
- (114) T. H. Le, Y. Kim, and H. Yoon, *Polymers (Basel)*, **9**, 150 (2017).
- (115) R. Gangopadhyay, B. Das, and M. R. Molla, *RSC Adv.*, **4**, 43912 (2014).
- (116) Z. Lu, M. Layani, X. Zhao, L. P. Tan, T. Sun, S. Fan, Q. Yan, S. Magdassi, and H. H. Hng, *Small*, **10**, 3551 (2014).
- (117) C. T. Hong, Y. H. Kang, J. Ryu, S. Y. Cho, and K. S. Jang, *J. Mater. Chem. A*, **3**, 21428 (2015).
- (118) C. J. An, Y. H. Kang, H. Song, Y. Jeong, and S. Y. Cho, *ACS Appl. Energy Mater.*, **2**, 1093 (2019).
- (119) D. S. Montgomery, C. A. Hewitt, R. Barbalace, T. Jones, and D. L. Carroll, *Carbon*, **96**, 778 (2016).
- (120) I. Petsagkourakis, K. Tybrandt, X. Crispin, I. Ohkubo, N. Satoh, and T. Mori, *Sci. Technol. Adv. Mater.*, **19**, 836 (2018).
- (121) H. J. Song, Y. Qiu, Y. Wang, K. F. Cai, D. L. Li, Y. Deng, and J. Q. He, *Compos. Sci. Technol.*, **153**, 71 (2017).

**Publisher's Note** Springer Nature remains neutral with regard to jurisdictional claims in published maps and institutional affiliations.